Department of Precision and Microsystems Engineering

Ride comfort optimization of a ropeless elevator

Koen Baron

Report no : 2018.016
Coach : Ir. Rik Schreurs
Coach : PhD. Hassan HosseinNia
Professor : Prof.Dr.Ir. Just Herder
Specialisation : PME
Type of report : Thesis
Date : 03-07-2018

Abstract

Tall buildings lose a big part of their expensive space to elevator shafts. A ropeless elevator reduces the amount of shafts, because multiple cabins are able to move in the same shaft.

Currently an elevator using a row of linear motors along the shaft is in the end phase of development. Tests on a full scale prototype have proven the concept. However vibrations in the current concept are over ten times higher than those in traditional elevators, resulting in an uncomfortable ride.

Actuators are placed over the length of the shaft, each one of them operating independently from its neighbors. Every single actuator contains its own position sensor, which was specifically designed for this application. With the measured position every actuator can apply a feedback force on top of the feed forward force. In theory a smooth vibration free ride is possible, but yet for unknown reasons vibrations exist.

The first objective of this research is to investigate the sources of vibration. With the knowledge obtained in this investigation, improvements are proposed and worked out. The final goal is to improve the comfort to an internationally accepted level.

Causes of vibrations are found. The dominant factors are the position sensor, the magnet yoke and the control algorithm. All position sensors will be calibrated, the tolerances of the magnet yoke can be compensated using a correction model and the controller is improved to fit the needs of the distributed actuation. The comfort is increased by a more than a factor ten, which brings it to a level equal to that of traditional elevators.

Contents

List of Figures

List of Tables

List of Listings

References

Referenced

[1] Title: Laying the foundation for today's skyscrapers
Author (Company): (San Francisco Chronicle)

[2] Title: Learn Who Invented the Elevator and More
Author (Company): Bellis, Mary (Inventors.about.com)

[3] Title: 2631-1, Mechanical Vibration and Shock-Evaluation of Human Exposure to Whole-Body Vibration-Part 1-General Requirements
(Company): ISO

[4] Title: ISO 8041 - Human response to vibration
(Company): Deutsches Institut für Normung

[5] Title: Organization IS, ISO 18738 - Measurement of ride quality
(Company): ISO

[6] Title: The vibration discomfort of standing persons: 0.5–16-Hz fore-and-aft, lateral, and vertical vibration, Journal of Sound and Vibration
Author: Olivier Thuong, Michael J. Griffin

[7] Title: Vibration and comfort: vertical and lateral motion in the range 0.5 to 5.0 Hz, ERGONOMICS
Author: C. CORBRIDGE, M. J. GRIFFIN

[8] Title: Discomfort from feeling vehicle vibration, Vehicle System Dynamics
Author: M. J. Griffin

[9] Title: Elevator ride comfort monitoring and evaluation using smartphones
Author: Yang Zhang, Xiaowei Sun, Xuefeng Zhao, Wensheng Su

[10] Title: A general survey on lift ride quality at public buildings of the Hong Kong special administrative region
Author (Company): K. K. Li, Andy M. T. Suen, Eddie W. K. Wu (Hong Kong Architectural Services Department)

[11] Title: H-infinity control of permanent magnet linear motor in transportation systems
Author: N. C. Cheung, Y.-R. Chen, and J. Wu)

[12] Title: Linear motor powered transportation: History, present status, and future outlook
Author: R. Hellinger and P. Mnich)

[13] Title: Tubular linear motor position detection by hall-effect sensors
Author: S. Pan, P. A. Commins, and H. Du

[14] Title: Position estimation of linear synchronous motor using hall-effect sensors and a mems accelerometer in 3rd International Conference on Systems and Control
Author: L. Baghli and B. Khouane

[15] Title: Analysis and Design of an Integrated Absolute Position Sensor for a Coreless Linear Permanent Magnet Actuator
Author (Company): S.A.M. Hurkmans (Eindhoven University of Technology)

[18] Title: Closed-loop position control of complementary and modular linear flux-switching permanent magnet motor
Author: Y. Zhang, R. Cao, Y. Jin, and K. Wang)

[19] Title: Torque ripple minimization of a novel modular stator switched reluctance motor based on direct instantaneous torque control
Author: Y. Hu, W. Ding)

[16] Title: Vertical-Vibration Control of Elevator Using Estimated Car Acceleration Feedback Compensation
Author (Company): Jun-Koo Kang and Seung-Ki Sul (IEEE)
Date: 2013-10

[17] Title: Vertical-Vibration Control of Elevator Using Estimated Car Acceleration Feedback Compensation
Author: Jun-Koo Kang, Seung-Ki Sul

[20] Title: H-infinity Comfort Optimization for Modular Linear Motor Transportation Systems
Author (Company): D. Markovic (Eindhoven University of Technology)

[21] Title: The Design of High Performance Mechatronics
Author: R Munnig Schmidt

[22] Title: Feedback systems
Author: Karl Johan Astrom

[23] Title: Exposed linear encoders
Company: Heidenhain Corporation,

[24] Title: Mobile Diagnosis QS 3, the mobile ride analyzer for elevators
Company: Henning

[25] Title: Linear Hall-effect sensor ICs with analog output
Company: Allegro Microsystems

1. Introduction

This chapter will start with a short history of the evolution of elevators followed by the definition of ride comfort, the theme of this research. The state of the art and prior research will be discussed before this chapter will conclude by stating the objective of this research.

1.1. Evolution of the elevator

The earliest known reference to an elevator is in the works of the Roman architect Vitruvius, who reported that Archimedes built his first elevator probably in 236 BC, [1]. But the first elevator that resembles the systems as seen today was built in 1835. An innovative crude steam-driven elevator called the “Teagle” was developed by the company Frost and Stutt in England. The elevator was belt-driven and used a counterweight for extra power, [2]. Years later after emergency brake systems had been fully developed, cable elevators became widely used in the taller buildings of the 20th century.

Nowadays it is hard to imagine a tall building without an elevator. Most modern elevators used for passenger transport use a similar system. A cabin is attached to one end of the cable and on the other end a contra weight is fixed. The cable is then driven by a motor. Velocities go up to over $20\,\mathrm{m/s}$ and capacities to 80 people per cabin.

As buildings become taller, a higher throughput is required. This can either be achieved by increasing the size or the velocity of the elevator, or more shafts can be placed next to each other. Velocity and size are limited by safety, efficiency and more factors. Shafts take up a significant amount of expensive floor area. Latest innovations include a twin elevator, allowing two cabins in one shaft, and world’s first ropeless elevator.

With the removal of the cable, multiple cabins can move in a single shaft. In combination with rotational platforms, which allow the cabins to go sideways, elevators go up in one shaft and down in another. However, where traditional elevators experience vibrations of around $0.15\,\mathrm{m/s^2}$ peak to peak, [16, 9]. This innovative cable free elevator is subjected to vibrations reaching over $1\,\mathrm{m/s^2}$, resulting in an uncomfortable ride. More on this in the next section, Section 1.2.

1.2. Ride comfort

Vibrations during a ride cause discomfort for passengers [6, 7, 8]. Optimizing that comfort is the objective of this research. Human sensitivity filters are provided by [4, 3], the latter will be used in this research to evaluate comfort. Acceleration measurements over constant velocity moves will be performed. The measured acceleration ripple, Figure 1.1b, is filtered by the human sensitivity filter, Figure 1.1a. Humans are most sensitive for vibrations between 3 and $25\,\mathrm{Hz}$, acceleration ripples with these frequencies will have a more dominant effect on the comfort.

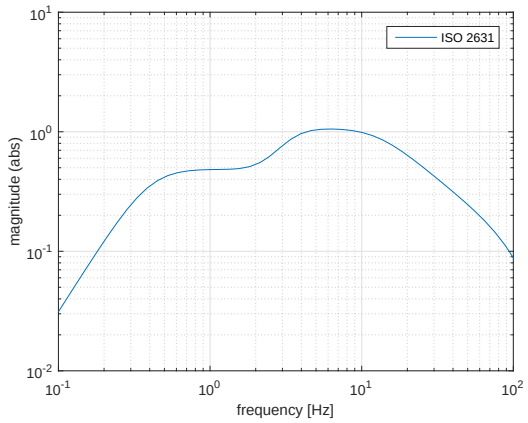

(a) Human sensitivity filter based on [3]

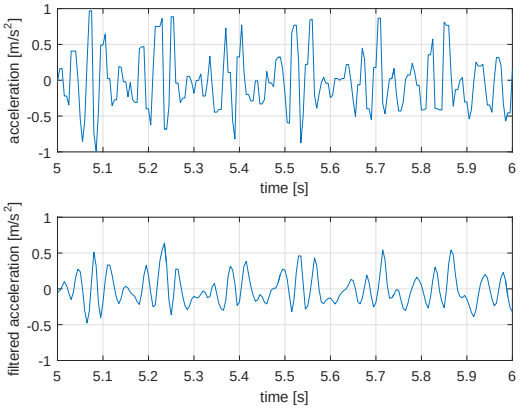

(b) Unfiltered and filtered acceleration during a $2\,\mathrm{m/s}$ move

After the acceleration measurement is filtered, the peak to peak values are analyzed. According to [5], discomfort can be defined as the A95 value, that is, 95% of the peak to peak values lie below this value, Figure 1.2. Ride comfort of traditional elevators have been measured [9, 10], A_{95} values around $0.15\,\mathrm{m/s^2}$ were found acceptable. This research only investigates vibrations in the direction of motion and dynamic behavior of the mechanics is left out of consideration. Therefore an A_{95} of $0.1\,\mathrm{m/s^2}$ will be considered acceptable. The comfort $\mathcal{C}$ is then defined in Equation (1.1). This means that a comfort level of one or higher will be acceptable.

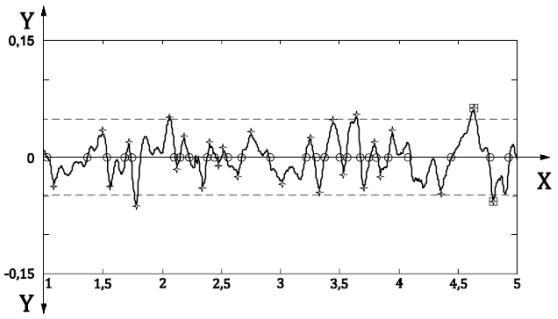

Key	
Y	vibration, $\mathrm{m/s^2}$
X	time, s
———	vibration
○	zero-crossing
✧	peak values
□	maximum peak-to-peak values
- - - -	A95 peak-to-peak values

Figure 1.2: Defining the A_{95} value according to [5]

$$\mathcal{C} = \frac{0.1}{A_{95}} \tag{1.1}$$

1.3. State of the art

A linear synchronous actuator is a suitable replacement for the cables, [11]. Linear direct drive systems have the advantage of being able to actuate multiple movers simultaneously, [12], thus increasing the throughput significantly.

A position sensor based on the Hall effect, [13, 14], is suitable for estimating positions in linear permanent magnet motors. In [15] a position sensor was designed for this elevator system. In order to operate individually every controller is equipped with this sensor.

A first full-scale prototype is built and the concept is proven, however acceleration ripples higher than $1\,\mathrm{m/s^2}$ exist and cause significant discomfort. Vibration control in traditional elevators is researched in [16, 17]. [18, 19] have researched control and comfort of modular motors, but the control is centralized. In [20] an H_∞ controller is proposed. It resulted in a complex controller suitable for just one operating velocity.

So prior to this research the comfort level is at a value of 0.2, Section 3.1, and the exact causes of vibrations are unknown.

1.4. Objective

Based on performances of traditional elevators and international standards a comfort value of 1 is set as the objective for this research. Other system requirements such as the position tracking error

should be compromised in order to achieve the desired comfort. In Tables 1.1 and 1.2 an overview of the relevant requirements and the goal is shown.

Table 1.1: Research objective

Parameter	Description	Min	Max	Unit
$\mathcal{C}$	Comfort level	1	-	

Table 1.2: Relevant requirements

Parameter	Description	Min	Max	Unit
$e_{pos,traj}$	Position tracking error at landing floor	-1	1	[mm]
$e_{pos,land}$	Position tracking error during trajectory	-100	100	[mm]
$e_{vel,traj}$	Velocity tracking error at landing floor	-0.005	0.005	[m/s]
$e_{vel,land}$	Velocity tracking error during trajectory	-0.1	0.1	[m/s]

1.5. Abbreviations

The use of abbreviations is minimized, but in some figures and tables they might occur. A list is given with those that can be found.

SC	System Controller
MC	Motor Controller
CU	Coil unit
MY	Magnet Yoke
PS	Position Sensor
FB	Feedback
FF	Feed Forward
PD	Proportional Derivative

1.6. Conventions

- z is the absolute position of the car or magnet yoke.
- v is the velocity of the car. Again positive is an upward motion or motion to the right depending on the orientation.
- s is the Laplace variable, used for equations in the frequency domain.
- When the position sensor is analyzed the magnet yoke position is a position relative to the sensor.
- Acceleration ripples are analyzed during constant velocity

2. System

An overview of the hardware is given in Figure 2.1 and a shematic overview in Figure 2.2. The system consists of the following elements:

- System controller
- Motor controller: motion control and current controller
- Coil unit: coils and position sensor
- Mover: magnet yoke which is connected to the cabin

Each of these parts will be discussed in this chapter.

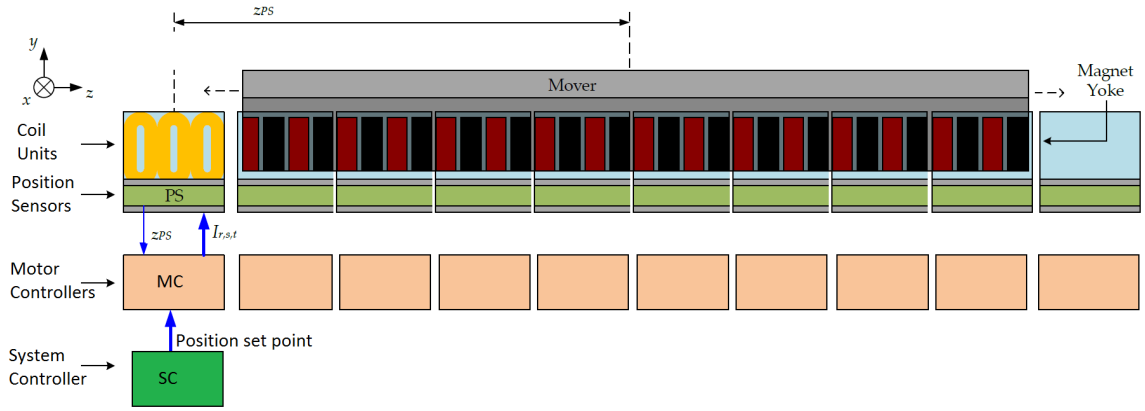

Figure 2.1: Overview of the hardware of the system

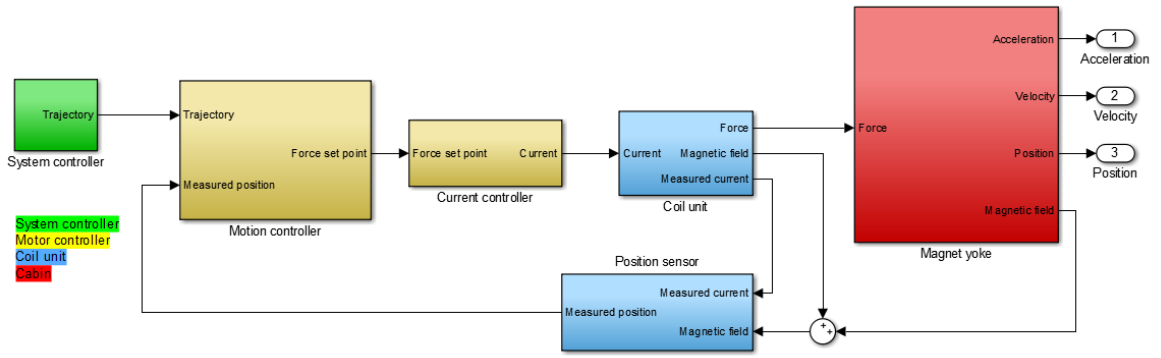

Figure 2.2: Schematic overview of connections between parts of the sytem

2.1. System controller

The system controller has two tasks. Generate a trajectory based on the users input and monitor the movement. It communicates this trajectory to every single motor controller. The trajectory is jerk, acceleration and velocity limited, the limits are found in Table 2.1. An example of a trajectory is shwon in Figure 2.3

Table 2.1: Third order motion profile limits

Symbol	Description	Value	Unit
j_{max}	Jerk limit	1.6	[m/s^3]
a_{max}	Acceleration limit	1.2	[m/s^{2}2]
v_{max}	Velocity limit	6	[m/s]

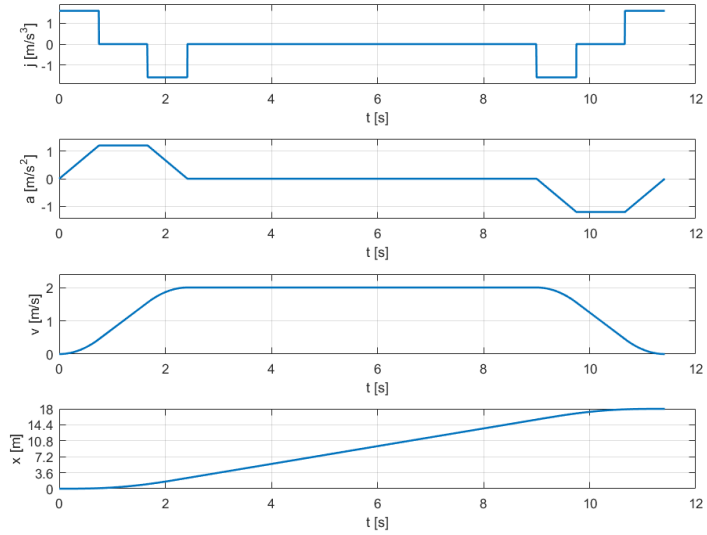

Figure 2.3: A third order motion profile with a maximum velocity of 2 m/s *move*

2.2. Motor controller

The motor controller receives a trajectory from the system controller and a position value from the position sensor. How much force needs to be applied is determined by the motion controller based on this information. A force set point is then transmitted to a current controller that applies the right amount of current. The bandwidth of the current controller is much higher than that of the motion controller and will therefore be considered as a constant gain of 1.

2.2.1. Motion control

A control loop is designed and implemented in the motor controller. It calculates the required force based on an input trajectory and a measured position value, Figure 2.4. The plant that is to be controlled will be discussed along with the important elements of the controller.

2.2.1.1. Car

For this research the car is modeled as rigid body with a constant mass, M_{tot}. Some damping is introduced by the guidance rail and eddy currents, D_{tot}. All other forces are modeled as disturbances, F_D. For this research the values of M_{tot} and D_{tot} are given in Table 2.4. Loads may vary in elevators, but it has been showed that this has a negligible effect on the acceleration ripple. For the position error the mass estimation error e_M does play an important role.

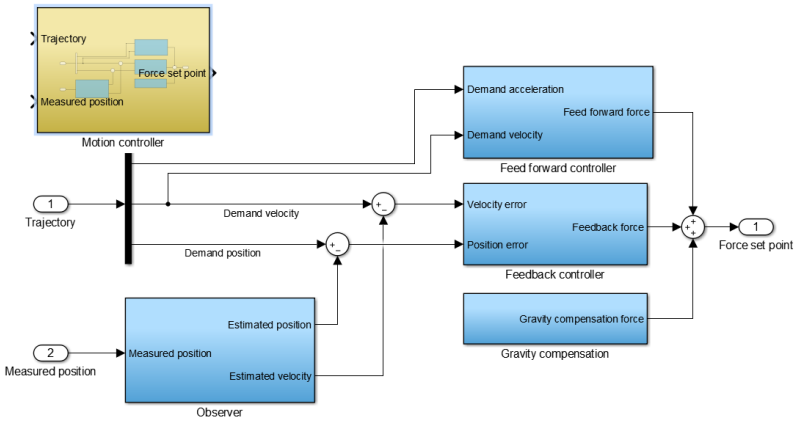

Figure 2.4: Schematic overview of the motion control

$$P(s) = \frac{1}{M_{tot}s^2 + D_{tot}s}z \tag{2.1}$$

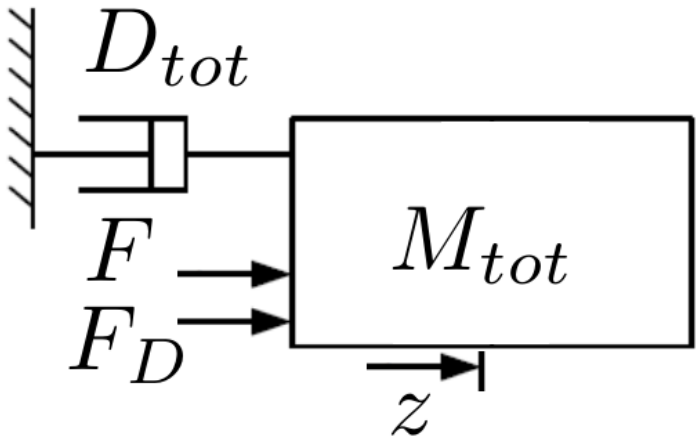

Figure 2.5: Dynamics of the car

Table 2.2: Relevant car parameters

Symbol	Description value	Unit	
M_{total}	Measured total mass	1200	[kg]
D_{tot}	Estimated total damping	105	[Ns/m]
e_M	Mass measurement error	10	[kg]

2.2.1.2. Feed forward controller and gravity compensation

A third order motion profile is generated by the trajectory generator and is used as a set point for the controller. Third order means jerk, acceleration and velocity limited, the limitations are stated in Table 2.1. The demand acceleration is multiplied by the measured mass M_m of the car, the demand velocity is multiplied by the estimated friction D_m, they form the feed forward force set point. If the elevator moves in vertical direction a gravity compensation force is added, F_g. Figure 2.3 shows an example of a motion profile, Equation (2.2) shows the calclution of the feedforward force.

$$F_{ff} = a_{ref} \cdot M_m + v_{ref} \cdot D_m + F_g \tag{2.2}$$

2.2.1.3. Feedback controller

A feed forward controller on a mass-damper system can not provide stability and is not able to deal with disturbances and uncertainties. So, every single motor controller has a feedback loop to obtain stability and better overall performance. Every individual controller is basically a PD controller. The control challenge is the small allowed position error during landing and the desired low acceleration ripple during motion. No intregral control is used because of the distributed nature of the system. To stay within the position limits during landing, the proportional gain is increased when the mover is reducing its velocity. During motion it is required to keep the gains low to have a smooth ride. The different gains and how the controller switch between gains will be discussed.

$$C(s) = K_p + K_d \cdot s \tag{2.3}$$

Departure and arrival

When the car starts its move the brakes are released. At this point it is desired that the car drops down less than 1 mm. With a mass measurement accuracy of ± 10 kg a certain static gain is needed to stay within that limit, Equation (2.4). Increasing K_D results in less overshoot, but will have a negative effect on the acceleration ripple in the landing window. It is found by tuning.

$$K_p > \frac{\Delta M * g}{e_{z_{land}}} = \frac{\mathbf{10 * 9.81}}{\mathbf{0.001}} = 9.81 \times 10^4 \,\mathrm{N/m} \tag{2.4}$$

Trajectory

During motion it is desired to keep the effect of noise on the position and velocity measurement as low as possible. Yet the tracking error should not become too great and stability needs to be maintained. The proportional gain is chosen to meet the tracking error condition, Equation (2.5), the differential gain to stabilize the controller.

$$K_p > \frac{\Delta M * g}{e_{z_{traj}}} = \frac{\mathbf{10 * 9.81}}{\mathbf{0.1}} = 9.81 \times 10^2 \,\mathrm{N/m} \tag{2.5}$$

Table 2.3: Car parameters

Symbol	Description	value
$K_P, traj$	Proportional gain during trajectory	2.5×10^4
$K_D, traj$	Differential gain during trajectory	3.8×10^4
$K_P, land$	Proportional gain during landing	3×10^5
$K_D, land$	Differential gain during landing	3.8×10^4

Control switching

Switching between landing and trajectory control, Figure 2.6, is based on the reference velocity. For velocities below Δv_{land} W_{land} is 1, between Δv_{land} and $\Delta v_{landrange}$ W_{land} decreases linearly. The feedback force, F_{fb} then follows from a linear combination of both controller outputs, F_{traj} and F_{land}, see Equation (2.6). The landing window does not influence the comfort as it is not within the constant velocity trajectory. It is however essential for meeting the requirement of the landing error.

$$F_{fb} = F_{traj} \cdot (1 - W_{land}) + Fland \cdot W_{land} \tag{2.6}$$

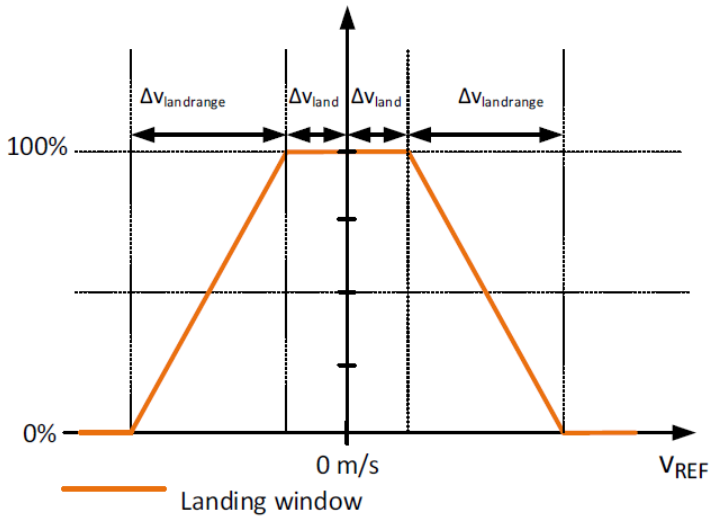

Figure 2.6: Switching between landing and trajectory control

2.2.1.4. Observer

The observer differentiates the measured position and finds a velocity. It can be modeled as a second order low-pass filter,

$$G_{obs}(s) = \frac{1}{\frac{1}{\omega_{co}^2}s^2 + \frac{2\zeta}{\omega_{co}}s + 1} \tag{2.7}$$

Table 2.4: Car parameters

Symbol	Description	value
ω_{co}	Cut off frequency of the second order low-pass filter	60 Hz
ζ	Damping ration of the filter	0.5

2.2.1.5. Distributed control

The control of the elevator is distributed over a large number of motor controllers. It is essential that handing over of the control is timed correctly. A windowing algorithm was designed to achieve smooth switching between controllers. A certain amount of overlap between the magnet yoke and the coil unit is desired before activating the coils. Not enough overlap will cause the motor control to generate more current, to achieve the same force as with full overlap. For efficiency and thermal reasons, the used current should be minimized. On the other hand, if only 7 out of 8 controllers are active, this means that they need more current to apply the same amount of force. While keeping these factors in mind, the windows were designed. Whenever there is a transition from 7 to 8 controllers, the other 7 will produce more force, this also requires perfect timing. Figure 2.7 shows exactly how a set of controllers switch and compensate as the magnet yoke passes.

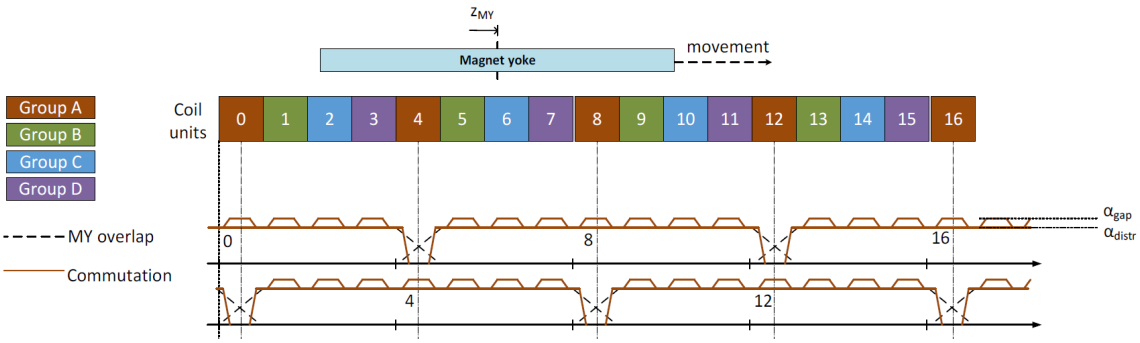

Figure 2.7: Windowing of motor controllers

When eight controllers are active, the controller force is multiplied by α_{dist}. When two controllers are handing over there is a brief moment, where only seven coil units are active, the gain is then increase to α_{gap}, Table 3.22

Table 2.5: Car parameters

Symbol	Description	value
α_{dist}	Distributed control gain	0.125
α_{gap}	Compensation gain	0.143

2.3. Coil unit

Current from the motor controller is transported to the coil units that are built along the shaft. Within these units three sets of coils can be found, one for each of the three phases. When the coils are placed perpendicular to a magnetic field, a Lorentz force, working on both the coils as well as the magnet, is the result. This is the driving force of the moving magnet yoke, Section 2.4.1. Movement of the magnet yoke results in a changing magnetic field, which is detected by the position sensor, located below the coils. The measured position sensor is then returned to the motor controller, which uses the measurement to calculate the new input currents.

2.3.1. Coils

Every coil unit contains three sets of coils, running a three phase current through these coils results a driving force of the mover. The frequency of the current depends on the velocity of the mover. Important dimensions of the coils are listed in Table 2.6 and Figure 3.4 gives an impression of the coil unit.

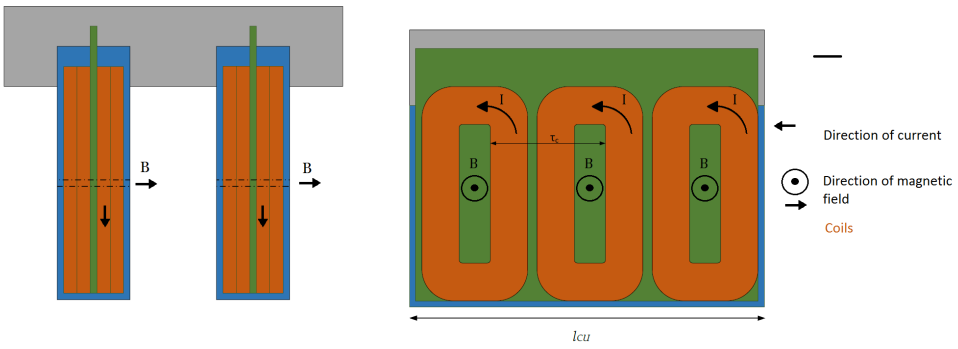

Figure 2.8: Front and side-view of a coil unit

Table 2.6: Coil unit dimensions

Parameter	Description	Value	Unit
l_{CU}	Length of single coil unit in direction of motion	300	mm
τ_c	Pitch between two adjacent coils	100	mm

2.3.2. Position sensor

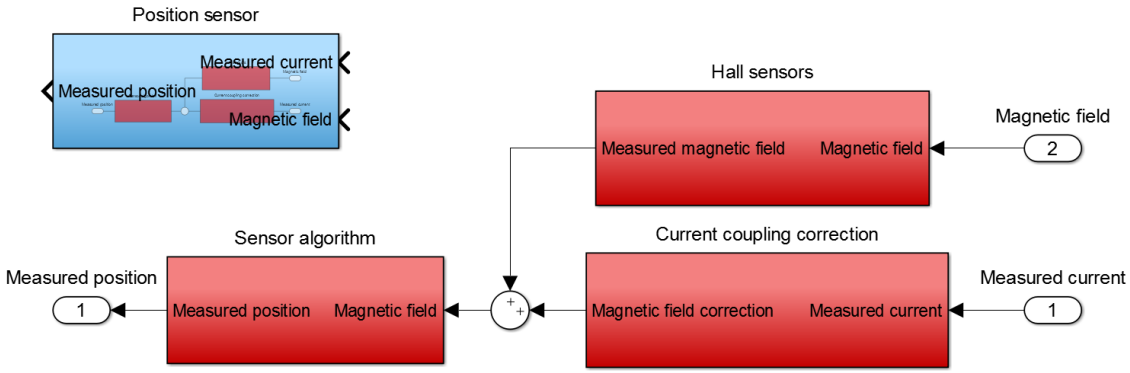

Figure 2.9: Schematic overview of the connections between components of the position sensor

A position sensor is required for commutation and feedback control. It was chosen to design a sensor that can be implemented in the coil unit in order to minimize cabling and installation time and costs. This is also beneficial from a control point of view, every coil unit has its own position sensor and is able to operate completely independent from others.

This position sensor was designed in [15] The sensor consists of 2 groups of 16 Hall sensors, Appendix A, both groups are again separated into two strips of 8 Hall sensors next to each other. A research has led to this optimal configuration, where position and magnetic tolerances have a minimal effect on the performance of the overall position sensor. It is also optimized for maximum range and minimal influence of the magnetic field induced by the coils. Of the 32 Hall sensors only 24 are being used in the current configuration. Figure 2.10 shows where the sensor is located with respect to the coils and magnets.

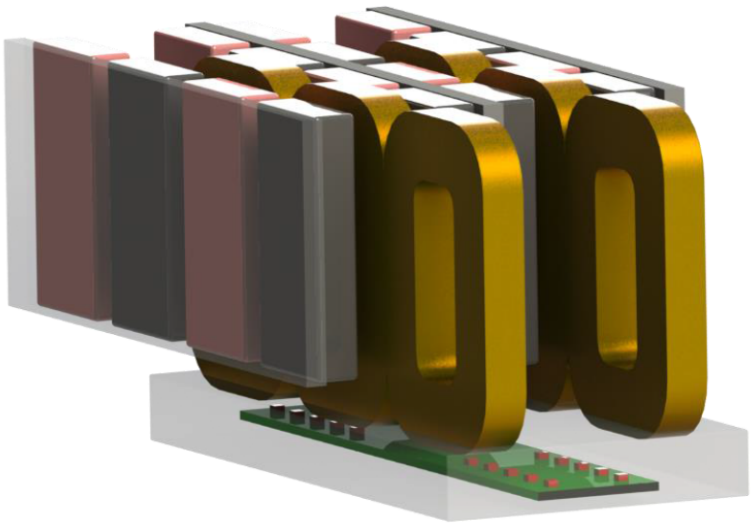

Figure 2.10: Coils, position sensor and magnet yoke combined

2.3.2.1. Sensor algorithm

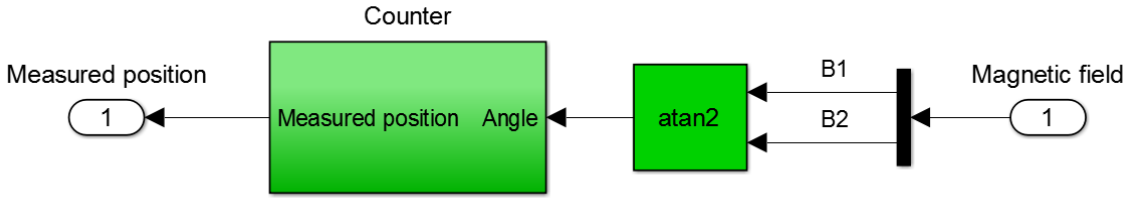

Figure 2.11: Schematic overview of the functions of the sensor algorithm

The sensor algorithm is based on two Hall sensors,Appendix A, more Hall sensors are used to increase accuracy and precision. This section will describe the steps of the algorithm that are relevant for this research, see Figure 2.13 for visual support.

1. The magnet yoke passes two Hall sensors that are half a magnet pole pitch apart
2. Each hall sensor measures the field strength, B1 and B2
3. The angle between the two signals is taken using the arctangens
4. A counter function detects jumps and constructs a position value

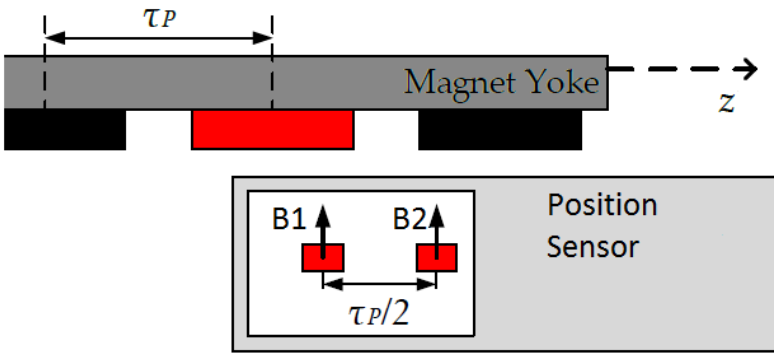

Figure 2.12: The magnet yoke passes two Hall sensors located half a pole pitch apart

2.3.2.2. Current coupling correction

A current through a coil generates a magnetic field. The hall sensors are placed on locations where the influence of this field is minimal, yet it is still present. In [15] a correction matrix was found using a finite element analysis, it was also validated to be correct up to 90%. Current sensors measure the current that is running through each coil, the magnetic field is then found by multiplying the current with the values of the correction matrix. This value is added to the measured field in order to approach the magnetic field of the magnet yoke alone, for high currents this significantly improves the performance of the position sensor.

$$B_{CU} = \begin{bmatrix} K_R & K_S & K_T \end{bmatrix} \cdot \begin{bmatrix} I_R \\ I_S \\ I_T \end{bmatrix} \tag{2.8}$$

For high payloads, big currents are required. If currents get too high, the system might become unstable, because the correction is imperfect. In Appendix E the loop gain at which instability occurs is evaluated.

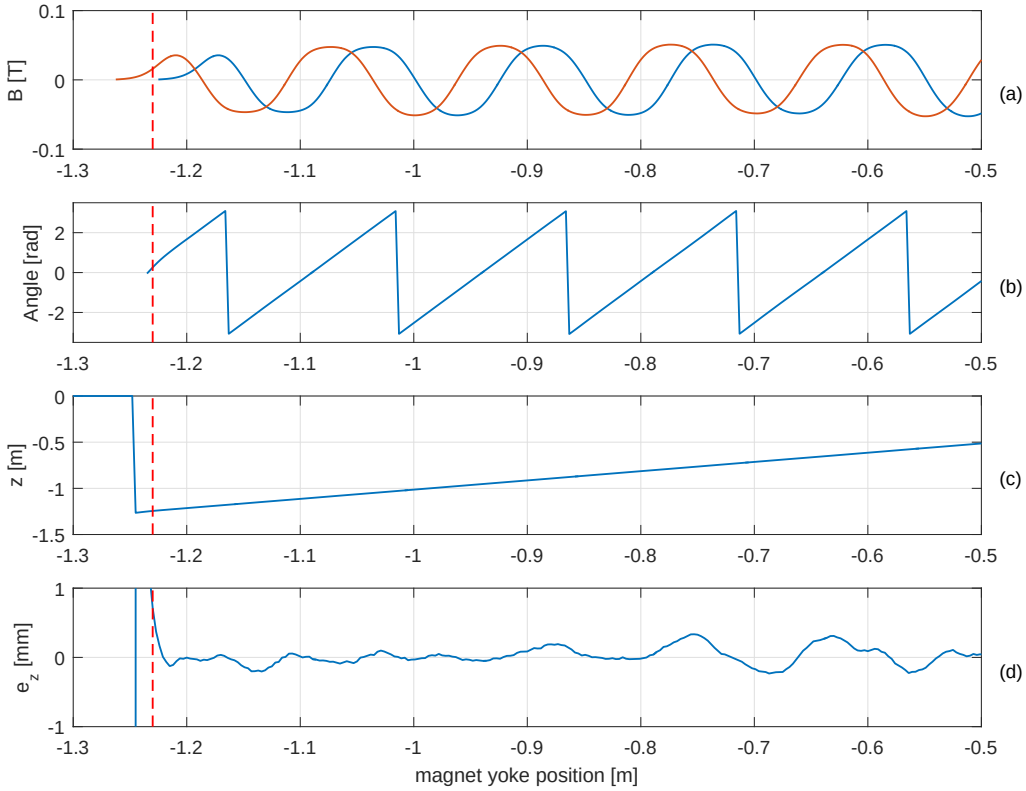

Figure 2.13: Position sensor algorithm. (a) two Hall sensors measure a passing magnet yoke. (b) the angle between two signals. (c) the angle is translated into a position using a counter function. (d) a small position error due to physical characteristics of the sensor.m

2.3.2.3. Performance

The performance of the sensor depends on the Hall sensors, but more importantly, on the magnets it measures. Also the amount of current flowing through the coils has a small influence, due to the imperfect correction. In Figure 2.14 a typical position error over the range of the sensor is shown and the specifications are given in Table 2.7.

Table 2.7: Position sensor specifications

Specification	Value	Unit
Range	[-1.23,1.23]	m
Precision	0.8	mm
Sampling frequency	8	kHz

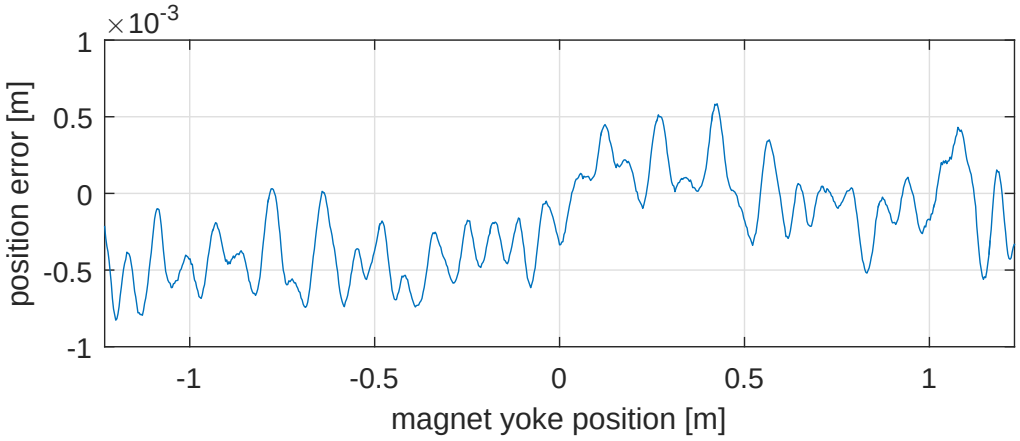

Figure 2.14: Typical error of the position sensor

2.4. Mover

The mover consists of a magnet yoke that is connected to a cabin, the dynamics of the cabin are not considered in this research. It can therefore be modeled as a rigid mass. On the horizontal test track, there is no cabin at all. The dynamic behavior of the cabin are not considered in this research. The mover is constrained for all translations and rotations by a set of wheels on a rail. Except for the friction they cause, they are assumed to have no influence on the system.

2.4.1. Magnet yoke

The magnet yoke is built out of several segments, Figure 2.15. Each segment contains a set of five magnets, two halves on the side and three wholes in between. It is designed to have maximum power density and minimum force ripple. The dimensions of the magnets are given in Table 2.8.

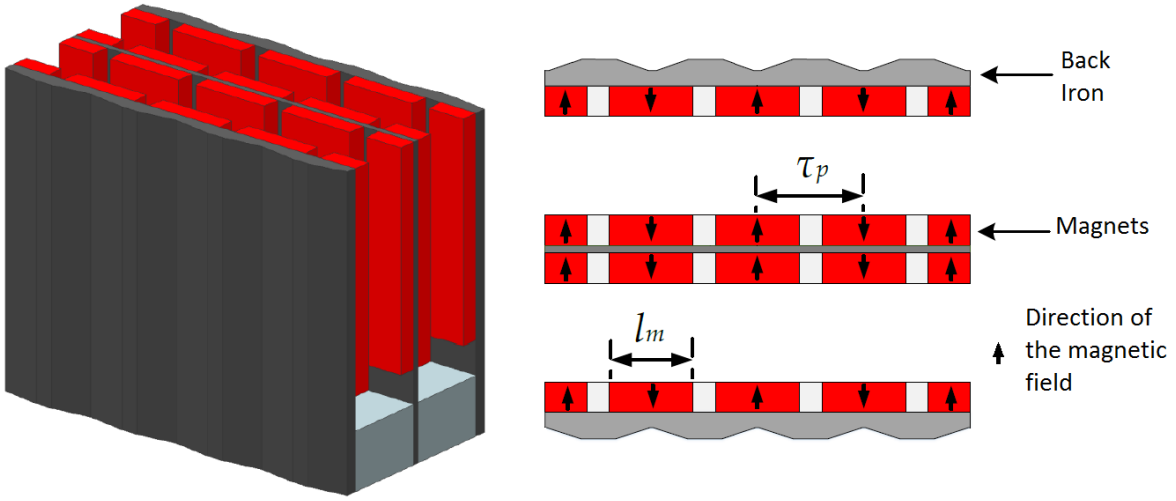

Figure 2.15: 3D and topview of one of the eight magnet yoke segments

Table 2.8: Relevant magnet dimensions

Parameter	Description	Value	Unit
l_m	Length of a single magnet in the direction of motion	60	mm
τ_p	Pitch between two adjacent magnet poles	75	mm

2.5. Test setups

Two test setups are used during this research, a horizontal and a vertical track. The differences are listed in table. Ideally everything is tested on the vertical test setup, but due to availability some tests have only been executed on the horizontal track. It is mentioned on which tracks tests are performed.

Table 2.9: Differences between two test setups

Parameter	Description	Value		Unit
Orientation	Direction of the movement	Vertical	Horizontal	
M_{total}	Total mass of the mover	1200	400	kg
l_traj	Maximum length of the trajectory	44	7	m
j_max	Maximum jerk	1.6	6.5	m/s^3
a_max	Maximum acceleration	1.2	5.5	m/s^2
v_max	Maximum velocity	6	3.5	m/s

2.5.1. Acceleration measurement

This research focuses on the discomfort caused by the propulsion system. Dynamic behavior of the cabin and of the wheels has an influence on the acceleration, but is not considered in this research. However, when an accelerometer is used to measure vibrations, these influences are also measured. Ideally the applied force is measured, because this is directly linked to the acceleration, Equation (2.9), if damping and disturbances are neglected. It is impossible to measure the applied force, therefore the force set point is used as a second method. If the transfer from force set point to applied force is equal to 1, the force set point is equal to the applied force.

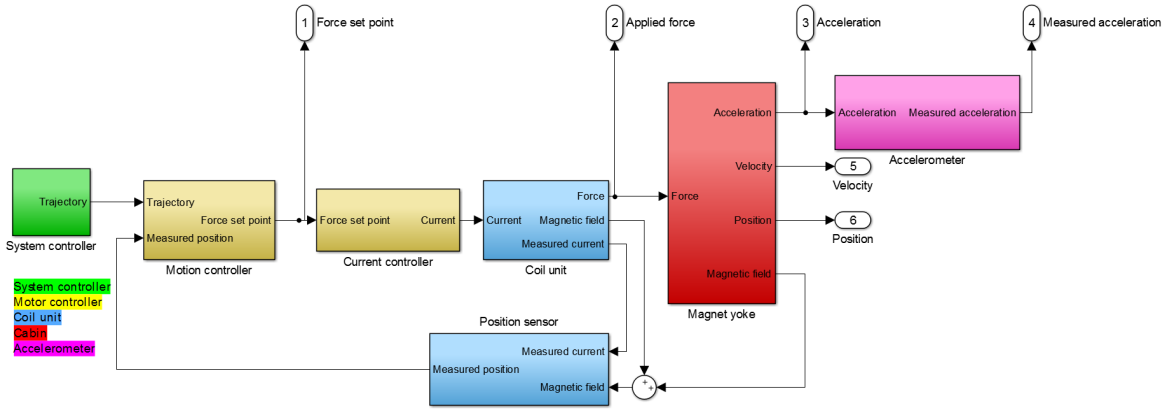

Figure 2.16: 3D and topview of one of the eight magnet yoke segments

$$a = \frac{F}{M} \tag{2.9}$$

In order to validate the assumptions that were made, the measurement of an accelerometer is compared with the force divided by the mass. Sections 2.5.1 and 2.5.1 show comparisons of the two methods at $2\,\mathrm{m/s}$ and $4\,\mathrm{m/s}$ respectively.

Figure 2.17: Comparison of two acceleration measurement on a move of $2\,\mathrm{m/s}$

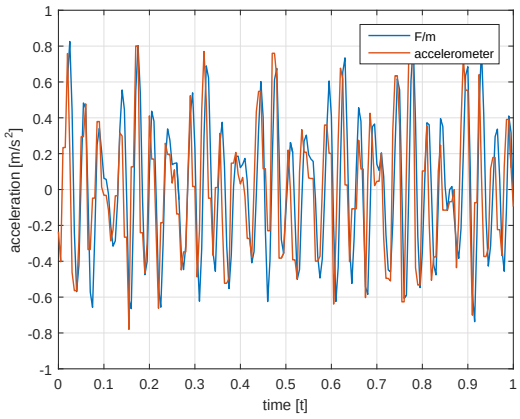

(a) Comparison at $2\,\mathrm{m/s}$

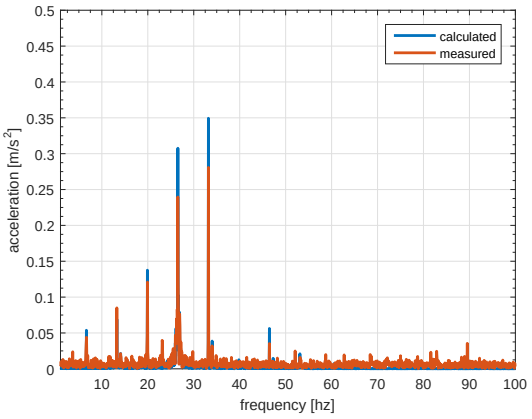

(b) Fourier transform of both results at $2\,\mathrm{m/s}$

For a move at $2\,\mathrm{m/s}$ the signals are almost equal, both in the time and frequency domain. At a velocity of $4\,\mathrm{m/s}$ it seems that the accelerometer is having difficulties in following the quick vibrations. In the frequency domain it becomes clear that the dominant frequencies are discovered with both methods, but more 'noise' is present on the accelerometers signal. This noise could come from the sensor, the wheels, the dynamic behavior of the cabin or from the motor characteristics. However since no

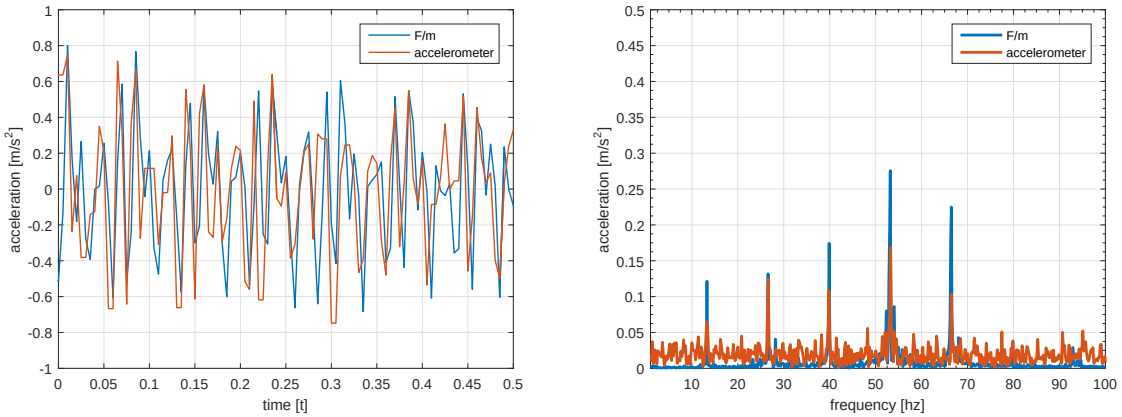

(a) Comparison at $4\,\mathrm{m/s}$ *(b) Fourier transform of both results at* $4\,\mathrm{m/s}$

Figure 2.18: Comparison of two acceleration measurement on a move of $4\,\mathrm{m/s}$

clear peaks are formed, it is assumed it is mostly sensor noise. It can therefore be concluded that using the force set point can be used as an acceleration measurement. For more details about the accelerometer, [24].

3. Development

This chapter covers the contribution of this research project. It is divided into three sections:

- Error analysis, the causes of vibration are investigated and quantified
- Calibration, the position sensor is improved by means of calibration
- Control, new control methods are proposed and validated

Validating solutions is done on either the horizontal track or the vertical track. The test for every concept consists of constant velocity moves at positive and negative velocities between 0.5 and $6\,\mathrm{m/s}$ with increments of $0.5\,\mathrm{m/s}$. On the horizontal track the maximum velocity is $3.5\,\mathrm{m/s}$. Moves at $2\,\mathrm{m/s}$ are chosen for comparison. They are compared with the baseline measurement unless otherwise mentioned. The comfort of the ride, defined in Section 1.2, is evaluated at every velocity and visualized in a plot. The average comfort is used as indication of the performance of solution, but in the end the comfort must be higher than 1 for all velocities, so the minimum value is just as important.

3.1. Error analysis

To improve the comfort of the elevator it is very important to know what is causing discomfort. In other words, which factors cause ripples in the acceleration and to what extent. The first step that is taken to get a better understanding in the source of the acceleration ripple, is a Fourier analysis on the acceleration ripple, Figure 3.1a. In Section 2.5.1 it was validated that both the acceleration measurement and the force set point can be used to find the acceleration ripple. In this section measurements are used for comparison, but force set point values will result in the same conclusions.

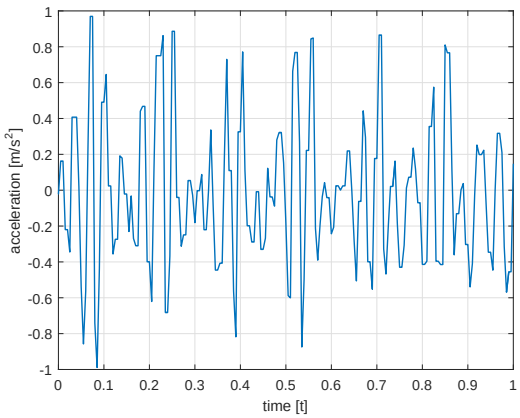

(a) Measured acceleration ripple

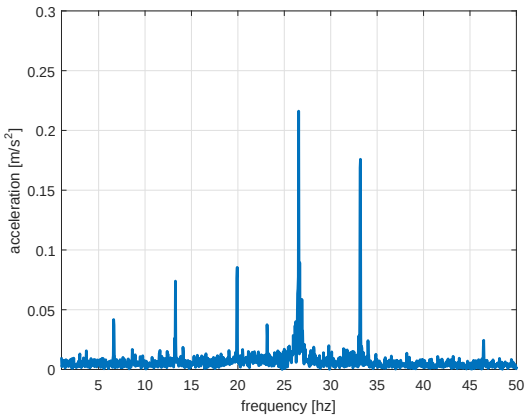

(b) Fourier transform of acceleration ripple

Dominant vibrations at certain frequency are clearly present. Because the measurement was performed at constant velocity, these frequencies correspond to typical dimensions of the system, .Sections 2.3 and 2.4.1 and Equation (3.1)

$$l = \frac{v}{f} \tag{3.1}$$

Based on these insights the components in Table 3.2 will be analyzed to gain quantitative knowledge of their contribution. A constant velocity move of $2\,\mathrm{m/s}$ is simulated in a model with distributed control and actuation. All tolerances, errors and deviations can be added individually. This makes it possible to investigate the influence of every single factor separately.

Table 3.1: Frequencies and their correspoding system components

Frequency [Hz]	Velocity [m/s]	Corresponding length [mm]	Corresponding component
6.7	2	300	Coil unit
13.3	2	150	Double pole pitch
20	2	100	Single coil
26.7	2	75	Pole pitch
33.3	2	60	Single magnet

Table 3.2: All components that are analyzed for their influence on the acceleration

Factor	Deviations
Current controller	settling of current controller
Coil units	variation in position ± 1 mm
Magnet yoke	variation in remanence ± 2%
Mass	variation in mass ± 30 kg
Damping	variation in damping · 10 ± 50 Nm/s
Position sensor	Bias, sensitivity, magnets and current coupling

3.1.1. Perfect model

First it is proven that no acceleration ripples are present when no tolerances are added to the model. The ripple and filtered ripple are shown in Figure 3.2 and the A_{95} value is given in Table 3.3.

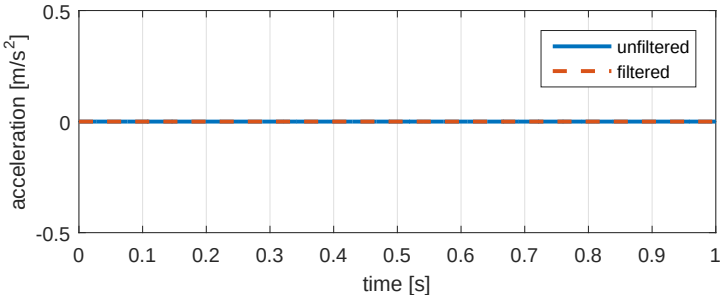

Figure 3.2: Acceleration ripples in a perfect model

Table 3.3: A_{95} for a perfect model

Factor	A_{95} [m/s^2]
Perfect model	0.00

As expected no ripple is present in a perfect model.

3.1.2. Current controller

The current controller is assumed to have a gain of 1. This assumptions is validated by running the simulation with a model of the current controller. Figure 3.3 shows the effect of the current controller on the acceleration ripple and the A_{95} value is given in Table 3.4.

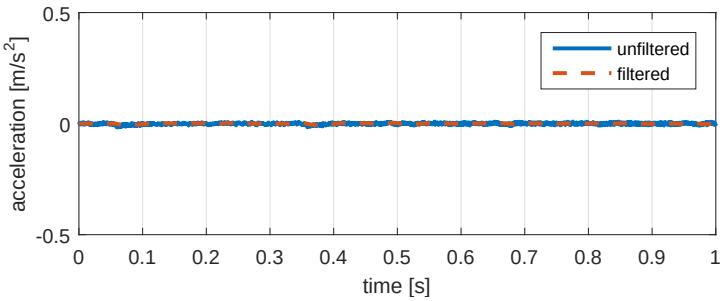

Figure 3.3: A_{95} caused by the current controller

Table 3.4: Filtered acceleration ripple due to the current controller

Factor	A_{95} [m/s^2]
Current controller	0.01

A negligible acceleration error is caused by the current controller. Therefore the current controller can be regarded as a gain with value 1.

3.1.3. Coil units

Every coil unit is given a random position offset with a standard deviation of 1 mm in the simulation. This value is higher than the mechanical tolerances of the system. The effect is presented in Figure 3.4 and the A_{95} value is given in Table 3.5.

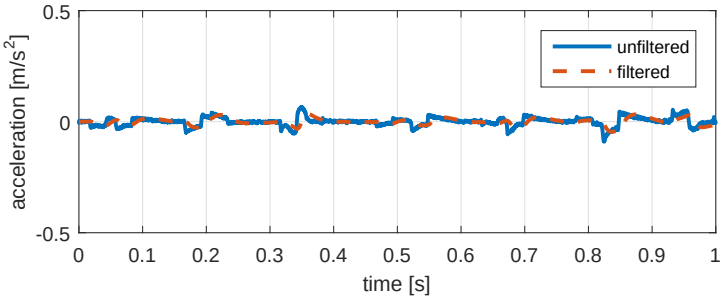

Figure 3.4: Filtered acceleration ripple due to the current controller and coil unit tolerances

Table 3.5: A_{95} caused by coil unit tolerances

Factor	A_{95} [m/s^2]
Current controller and coil unit tolerances	0.04

Even though the simulated deviations are higher than in the real system, the contribution to the acceleration ripple is still small.

3.1.4. Magnets

The mover is a magnet yoke made up of different magnets, Section 2.4.1. Tolerances are modeled as a random change in the theoretical motor constant with a standard deviation of 2%. Figure 3.5 shows the effect on the acceleration ripple and the A_{95} value is given in Table 3.6.

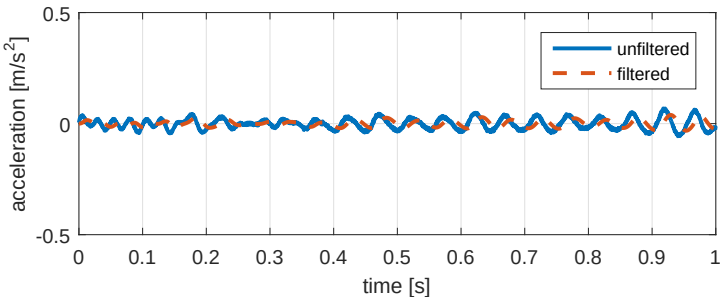

Figure 3.5: Filtered acceleration ripple due to the current controller and magnet yoke tolerances

Table 3.6: A_{95} caused by magnet yoke tolerances

Factor	A_{95} [m/s^2]
Current controller and magnet yoke tolerances	0.07

3.1.5. Mass estimation

A mass sensor measures the weight of car including the payload before a move. Feed forward and feedback force are based on the value of this measurement. The sensor can have an error between -30 and $30\,\mathrm{kg}$. This is simulated and the A_{95} is showed in Table 3.7

Table 3.7: A_{95} caused by a mass estimation error

Factor	A_{95} [m/s^2]
Mass overestimation, + 30 kg	0.00
Mass underestimation- 30 kg	0.00

3.1.6. Damping uncertainty

The damping was found by averaging the applied force at a constant velocity, it is $105\,\mathrm{Ns/m}$. In this experiment a variation in the form of white noise with an amplitude of $50\,\mathrm{Ns/m}$ is added. Also the effect of more and no damping is analyzed. The A_{95} of the worst case can be found in Table 3.8.

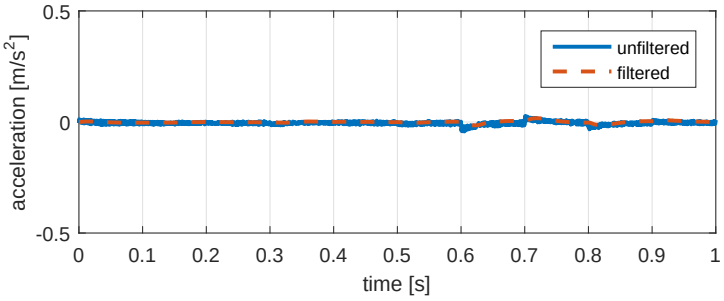

Figure 3.6: Filtered acceleration ripple due to damping uncertainty of factor 10 and variation

Table 3.8: A_{95} caused by damping uncertainty

Factor	A_{95} [m/s^2]
Damping variation, ± 50 Ns/m	0.03
Damping × 0	0.00
Damping × 10	0.00
Damping × 10 plus variation, ± 50 Ns/m	0.04

3.1.7. Control

The effect of the feedback is analyzed when no errors are present. The A_{95} can be found in Table 3.9.

Table 3.9: A_{95} caused by the controller

Factor	A_{95} [m/s^2]
PD controller, bandwidth 5 Hz	0.00

3.1.8. Position sensor

The acceleration ripple caused by the position sensor, is compared with that of an alternative sensor, [23]. Figures 3.7a and 3.7b shows the comparison in the time and frequency domain.

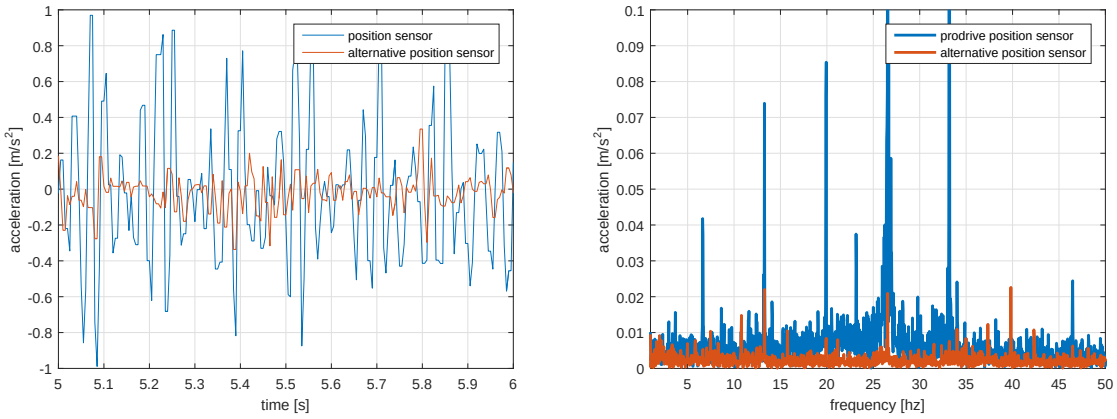

(a) Measured acceleration ripple

(b) Fourier transform of acceleration ripple

Figure 3.7: Acceleration ripple and fourier transform using two different sensors

This comparison makes it clear that the used position sensor is a dominant factor in the acceleration ripple. There are a couple of factors influencing the performance of the sensor, the most dominant are:

- Hall sensor sensitivities
- Hall sensor bias
- Magnet yoke
- Current coupling

A model of the position sensor is used to investigate how much each of these factors contribute to the position error of the sensor. Then the acceleration ripple caused by these position errors will be quantified.

3.1.8.1. Hall sensor sensitivities

Table 3.10 shows one set of measured Hall sensor sensitivities. These values are used to simulate the effect of Hall sensor sensitivities on the final position value. The effect is shown in Figure 3.8 and the contribution to the position error is shown in Table 3.11.

Table 3.10: Measured relative sensitivities used as input for the simulation

SG0		SG1		SG2		SG3	
HS	S [-]	HS	S [-]	HS	S [-]	HS	S [-]
1	1,03	1	0,98	1	1,03	1	1,03
2	1,00	2	1,02	2	1,00	2	1,00
3	1,00	3	1,01	3	0,98	3	1,01
4	1,01	4	1,01	4	0,98	4	0,98
5	0,98	5	1,00	5	0,99	5	0,96
6	0,99	6	1,00	6	0,98	6	1,02
7	0,99	7	1,02	7	1,01	7	0,96
8	0,99	8	0,98	8	1,03	8	1,04

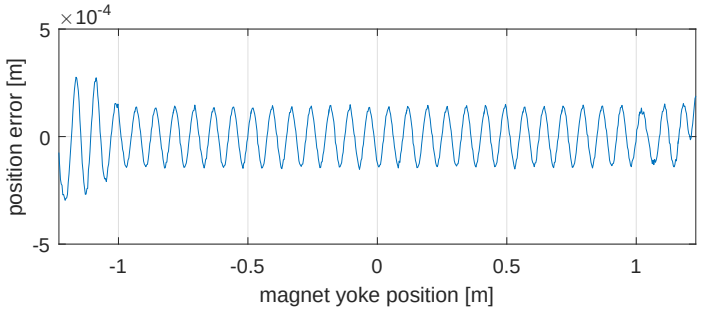

Figure 3.8: The position error due to the different Hall sensor sensitivities

Table 3.11: Contribution to the position error of the Hall sensor sensitivities

Factor	Position error [mm]	pitch [mm]
Hall sensor sensitivities, worst case	0.15	7.5

3.1.8.2. Hall sensor bias

Table 3.12 shows one set of measured Hall sensor biases. These values are used to simulate the effect of Hall sensor biases on the final position value. The effect is shown in Figure 3.9 and the contribution to the position error is stated in Table 3.13.

Table 3.12: Measured biases used as input for the simulation

SG0		SG1		SG2		SG3	
HS	B [mT]	HS	B [mT]	HS	B [mT]	HS	B [mT]
1	0.52	1	0.23	1	0.29	1	0.13
2	0.30	2	-0.02	2	0.42	2	0.04
3	0.40	3	0.21	3	0.23	3	0.10
4	0.32	4	0.20	4	0.32	4	0.16
5	0.15	5	0.22	5	0.42	5	0.15
6	0.34	6	0.28	6	0.40	6	0.24
7	0.05	7	-0.04	7	0.51	7	0.20
8	0.37	8	0.11	8	0.40	8	0.22

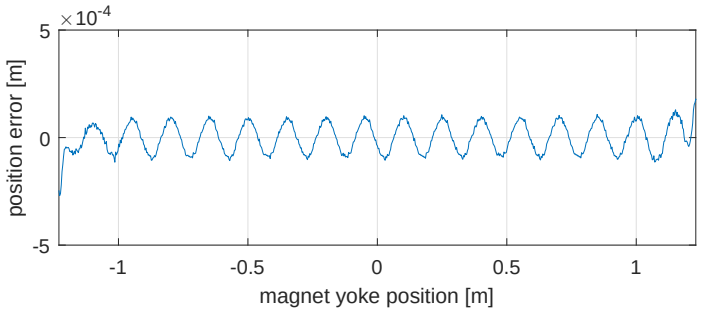

Figure 3.9: The position error due to the different Hall sensor biases

Table 3.13: Contribution to the position error of the Hall sensor biases

Factor	Position error [mm]	pitch [mm]
Hall sensor biases, worst case	0.08	15

3.1.8.3. Magnet yoke tolerances

Tolerances of the magnet yoke cause deviation in the actuator, but also in the sensor. The position error caused by the magnet yoke tolerances is obtained in Section 3.2.3. The contribution to the final error is stated in Table 3.14.

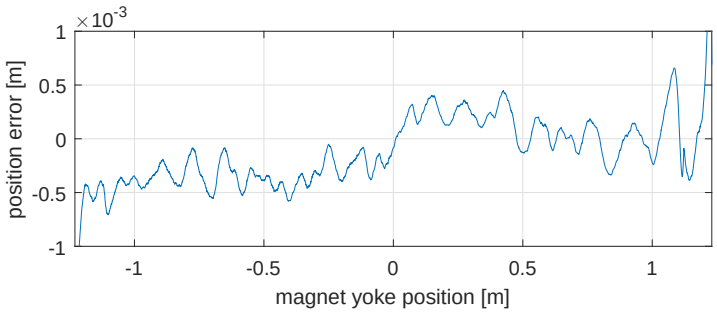

Figure 3.10: The position error due to the magnet yoke tolerances

Table 3.14: Contribution to the position error of the magnet yoke tolerances

Factor	Position error [mm]	pitch [mm]
Magnet yoke tolerances	0.7	15, 7.5

3.1.8.4. Current coupling

Prior research has shown that the magnetic field caused by the induction of the coil can be corrected up to 90%, [15]. The remaining 10% causes a position error depending on the current, this can lead to instability, Appendix E. It is analyzed how big the position error is due to a current of 60 A. A position sensor is influenced by the coils of its own coil unit, Figure 3.11 and the coils of the neighboring coil unit, Figure 3.12.

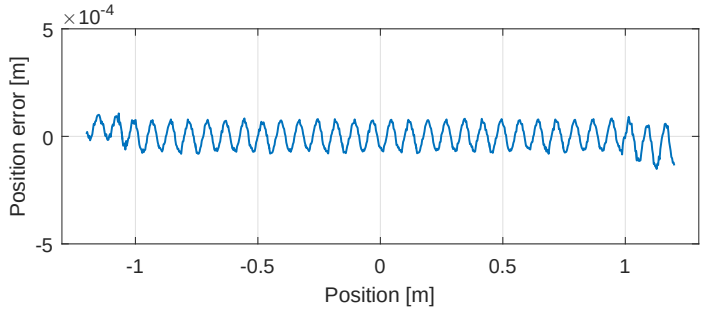

Figure 3.11: Position error due to a coupled current of 60 A *of its own coils*

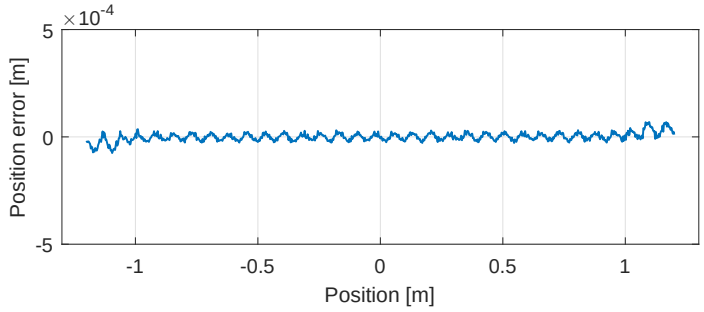

Figure 3.12: Position error due to the coupled current of 60 A *of the neighboring coil unit*

Table 3.15: Contribution to the position error of current coupling at 60 A

Factor	Position error [mm]	pitch [mm]
Current coupling	0.08	7.5

The error caused by neighboring coil units is much smaller than the other factors and is therefore left out of consideration.

3.1.8.5. Acceleration error due to the position error

Figure 3.13 shows an overview of all contributions to the position error of the sensor.

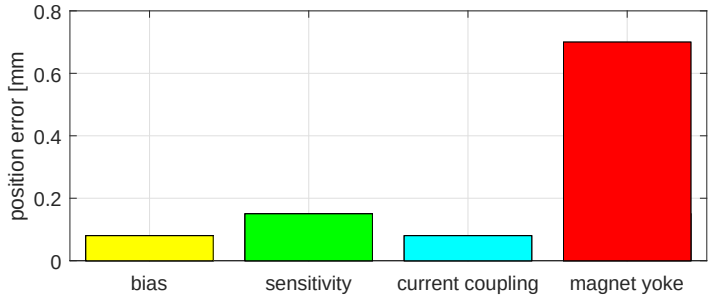

Figure 3.13: Filtered acceleration ripple due to position error while using only feed forward control

The magnet yoke tolerances are biggest contributor, but the other factors are not negligible. These errors are used in a simulation of a move of $2\,\mathrm{m/s}$ and the found A_{95} are stated in Table 3.16. The effect of the position sensor on commutation is obtained by simulating without feedback control, Figure 3.14. With feedback is presented in Figure 3.15.

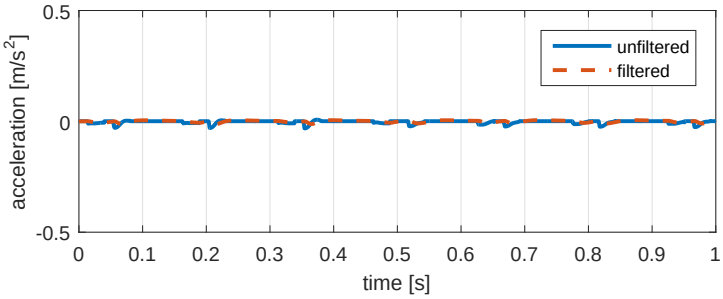

Figure 3.14: Filtered acceleration ripple due to position error while using only feed forward control

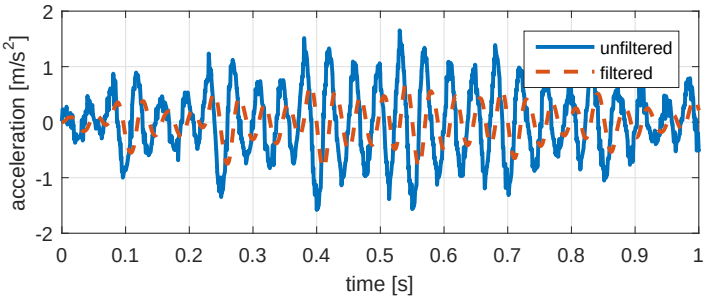

Figure 3.15: Filtered acceleration ripple due to position error while using feed forward and feedback control, note the change in scale compared to the previous plots

Table 3.16: A_{95} value caused by different factors of the position sensor

Factor	A_{95} [m/s^2]
Position sensor - HS bias, feedback	0.41
Position sensor - HS sensitivity, feedback	1.09
Position sensor - Current coupling (60 A), feedback	0.37
Position sensor - magnet yoke error, feedback	0.67
Position sensor - all errors, feed forward	0.02
Position sensor - all errors, feedback	1.54

3.1.9. Conclusion

All dominant contributions to the acceleration are gathered in Table 3.17 and represented graphically in Figure 3.16.

Table 3.17: A_{95} of dominant factors

Factor	A95peak [m/s^2]
Coil unit tolerances	0.04
Magnet yoke tolerances	0.07
Damping × 10 plus variation, ± 50 Ns/m	0.04
Position sensor, all errors, feedback	1.54

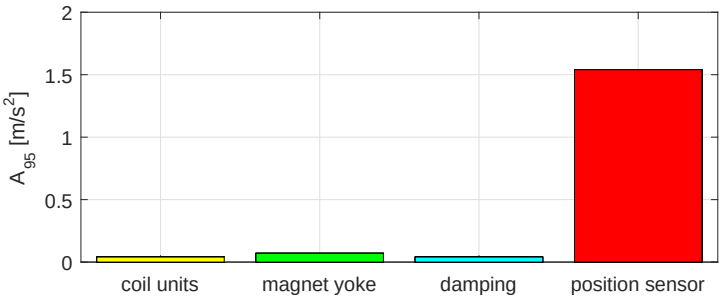

Figure 3.16: A visualization of the contributions to the acceleration ripple

Figure 3.17 shows a comparison of the simulated and measured acceleration ripple in the frequency domain. Peaks are located on the same frequencies, the amplitude is higher in the simulation is higher because a worst case position error is used for all sensors. On the prototype errors are not all as big as the worst case. Another reason is the effect of the accelerometer. The resemblance between the simulation and measurement indicates that the position sensor, when used in the feedback loop, is the most dominant source of the acceleration ripple. There are two methods of dealing with this. One is improving or changing the sensor, and the other is improving the controller. Both methods will be discussed in the Sections 3.2 and 3.3.

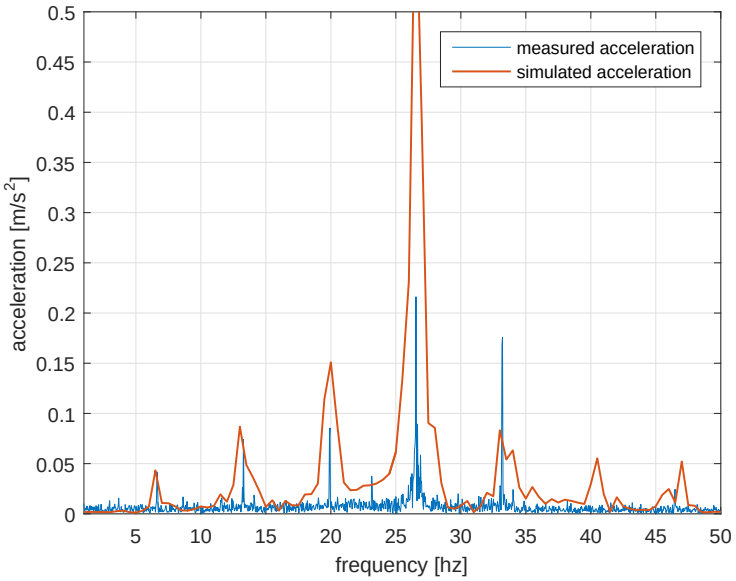

Figure 3.17: Comparison of the simulated and measured acceleration ripple in the frequency domain

3.2. Position sensor calibration

In Section 3.1 it was found that the position sensor's error leads to acceleration ripples when used in a feedback loop. Problems with sensor noise are best approached by finding the roots of the noise and trying to eliminate them, [22]. The causes were found, this section will discuss methods of noise elimination.

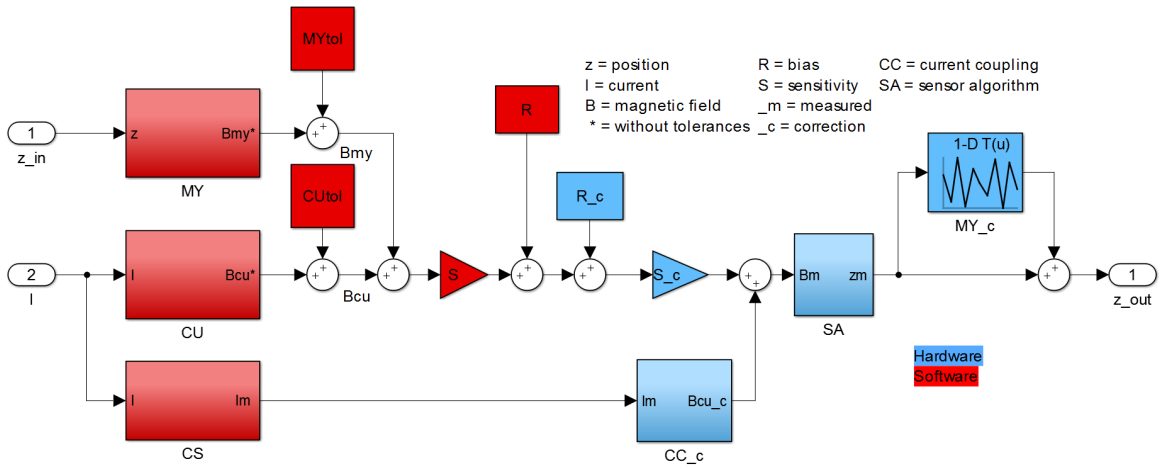

Figure 3.18: A model of how the sensor can be calibrated

A complete calibration of the sensor is proposed, a model is shown in Figure 3.18. Its aim is to minimize the position error, Equation (3.2), by eliminating all influencing factors. Equation (3.3) shows a mathematical representation of the calibration model shown in Figure 3.18.

$$e_z = z_{in} - z_{out} \tag{3.2}$$

$$((B_{MY} + B_{CU}) \cdot S + R + R_m) \cdot S_m + B_{CU_c} = Bm \tag{3.3}$$

If the correction values meet the following conditions:

$$R = -R_c \quad S = S_c^{-1} \quad B_{CU} = -B_{CU_c} \tag{3.4}$$

Then the measured magnetic field is equal to the magnetic field of the magnet yoke. Also the remaining position error is the difference between the magnet yoke correction and the effect of the magnet yoke tolerances:

$$B_{MY} = B_m \tag{3.5}$$

$$SA(B_{MY} + MY_{tol}) + MY_c = z_{out} \tag{3.6}$$

And if the correction model cancels the effect of the magnet yoke tolerances:

$$SA(MY_{tol}) = -MY_c \tag{3.7}$$

Then the position error is zero:

$$z_{in} = z_{out} \quad e_z = 0 \tag{3.8}$$

Because the erroneous position value is used as an input for the lookup table the correction will always be slightly off. But because the ratio between rate of change of the error and the small input error, it is possible to apply this method of correction, **??**

In this section an attempt is made to realize these conditions and bring the error as close to zero as possible. The improved comfort achieved with this calibration will be compared to the baseline comfort.

3.2.1. Hall sensor calibration

With two algorithms, Appendix C, the bias and sensitivity of every Hall sensor of every position sensor is obtained. The bias is found with a standard deviation of $0.02\,\mathrm{mT}$ and the relative sensitivity with a standard deviation of 1.8×10^{-3}. These values are implemented in the sensors software.

Calibrating the Hall sensors also indirectly improve the current coupling correction.

After implementation the remaining error is almost equal for all position sensors, Figure 3.19. This indicates that the magnet yoke is the cause for this error.

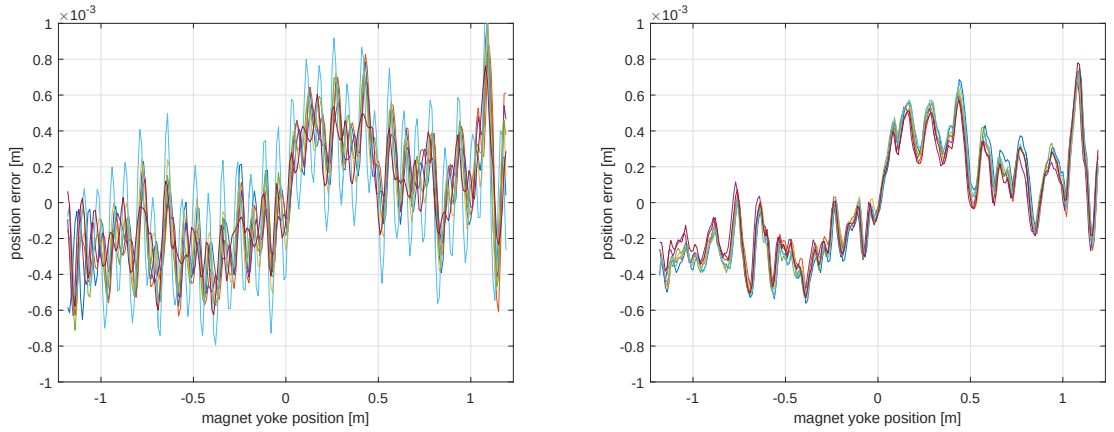

(a) Position error of 7 sensors

(b) Position error of 7 sensors after calibration

Figure 3.19: Result of the sensor calibration

3.2.2. Comfort

The position sensors are calibrated, what effect does this have on the comfort? Figure 3.20 shows the difference in filtered acceleration. A move of $2\,\mathrm{m/s}$ is chosen to use as comparison.

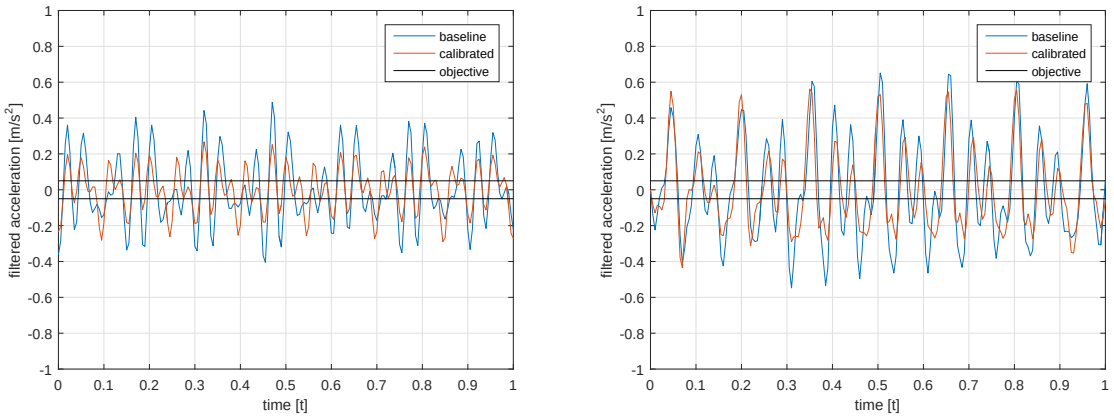

(a) Vertical track

(b) Horizontal track

Figure 3.20: Filtered acceleration before and after calibration

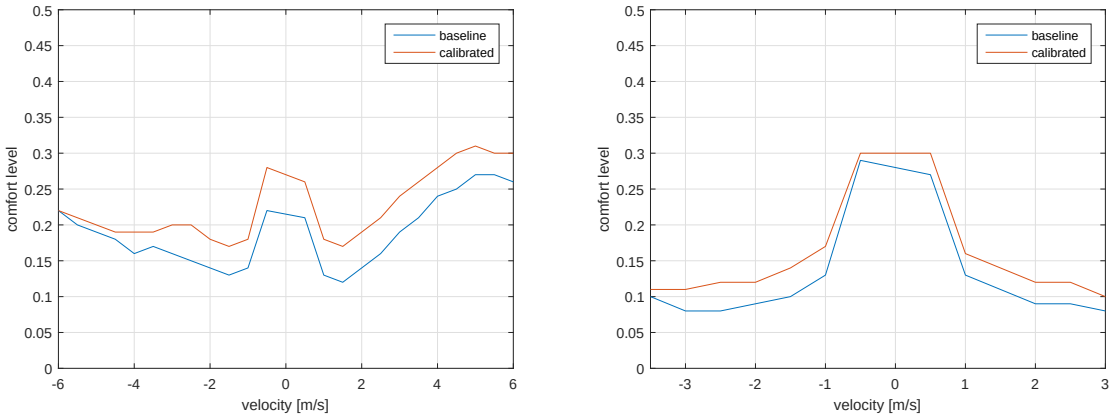

(a) Vertical track *(b) Horizontal track*

Figure 3.21: Comfort levels before and after calibration at different velocities on both tracks

Table 3.18: Average comfort level of the baseline before and after calibration on the vertical track

	Comfort level		
Configuration	Min	Average	Max
Baseline	0.12	0.19	0.27
Calibrated	0.17	0.23	0.31

3.2.3. Magnet yoke correction

A lookup table is made from the data of a set of position sensors. Because of a limited amount of available memory and the large quantity of different magnet yokes, the correction model should not be bigger than 50 data points. The model therefore only contains the position and value of the maximum absolute position errors, Figure 3.22a. An interpolation algorithm creates a third order polynomial between two points of the lookup table and reduces the position error significantly, Figure 3.22b.

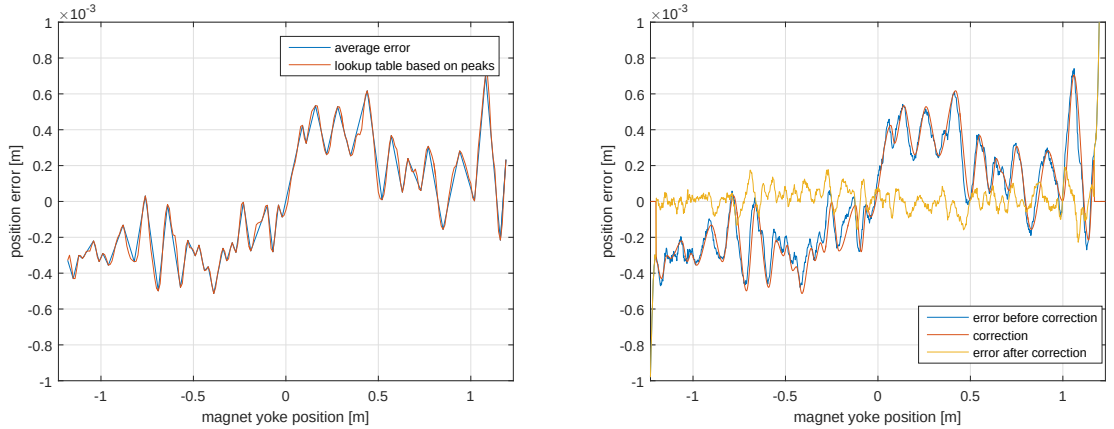

(a) Lookup table based on the peaks *(b) The position error before and after the correction*

Figure 3.22: Maximum position error is reduced to 0.2 mm

The maximum position error before calibration and magnet yoke correction was 0.8 mm. Now it is 0.2 mm, this is an improvement of 75%.

3.2.3.1. Comfort

The magnet yoke correction is only tested on the horizontal track. Acceleration values are shown in Figure 3.23 with and without calibration.

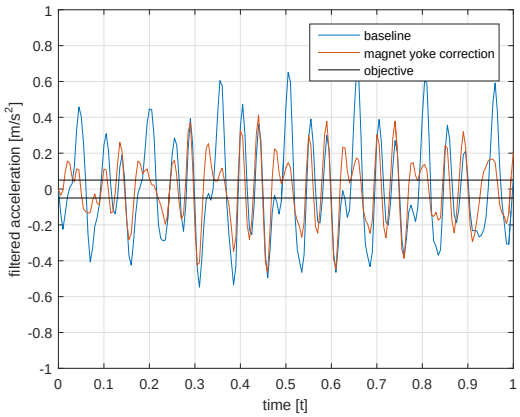

(a) Without calibration

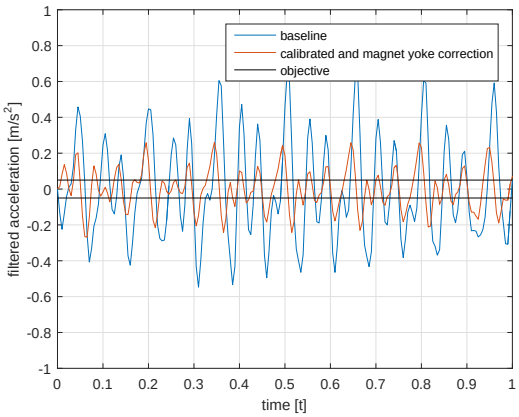

(b) With calibration

Figure 3.23: Filtered acceleration before and after calibration and magnet yoke correction

Correction of the magnet yoke is especially successful when the position sensors are calibrated, which is expected. The comfort levels for different velocities are shown in Figure 3.24.

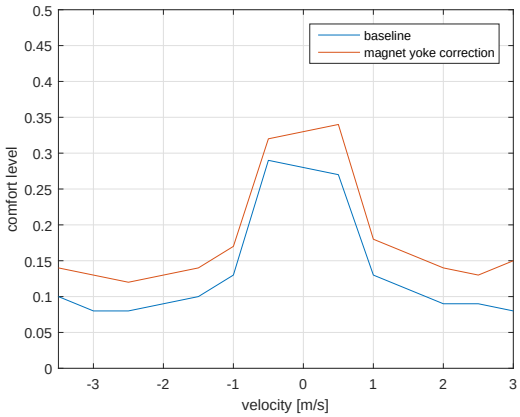

(a) Without calibration

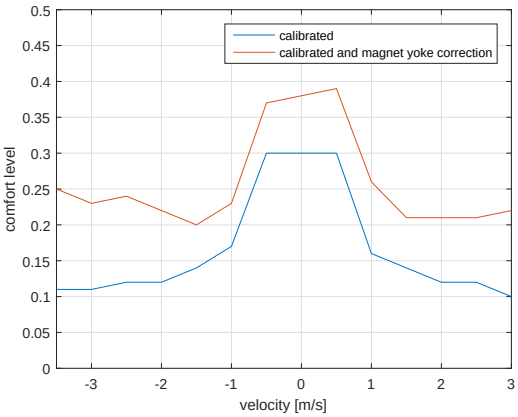

(b) With calibration

Figure 3.24: Comfort levels before and after magnet yoke correction

Table 3.19 shows the average and extreme values of all calibration methods.

Table 3.19: Comfort level of all calibration methods on the horizontal track

	Comfort level		
Configuration	Min	Average	Max
Baseline	0.08	0.12	0.29
Calibrated	0.10	0.15	0.30
Magnet yoke correction	0.12	0.17	0.33
Calibrated and magnet yoke correction	0.20	0.25	0.39

3.3. Improvements of the controller

In Chapter 2, the controller as it was used before is described. In this section knowledge obtained in the error analysis will be used to develop a new controller and then test it. Improvements will be made in the following control elements:

- PD control
- Low-pass filter
- Distributed control

This section will end with a final optimized controller that has been tested on the horizontal track.

3.3.1. PD control

Section 3.1 has shown that sensor noise is the most dominant contributor to discomfort. Solutions to improve the sensor's performance have been successful. But some noise will remain and it is the controller's task to deal with this. Equations (3.10) to (3.12) and (D.1) show the important transfer functions of the original controller. The sensitivity shows the relation between noise and position error, which is not relevant for the comfort. Complementary sensitivity describes the ratio between disturbance and the position error, again the position error is not the main issue in this research, Appendix B Sensor noise is the most dominant source of vibration, so the noise sensitivity will be analyzed, Figure 3.28b. It shows the transfer from noise (n) to controller output, force (F). And because of the low damping compared to mass, acceleration is by approximation directly proportional with the force.

$$P(s) = \frac{1}{Ms^2 + Ds} \tag{3.9}$$

$$C(s) = (Ms + D) \cdot 5 \cdot 2\pi \cdot \frac{1}{\frac{1}{\omega_{co}} s^2 + \frac{\zeta}{\omega_{co}} + 1} \tag{3.10}$$

$$L(s) = C(s)P(s) = \frac{10\pi}{s} \cdot \frac{1}{\frac{1}{\omega_{co}} s^2 + \frac{\zeta}{\omega_{co}} + 1} \tag{3.11}$$

$$CS(s) = \frac{F}{n} = \frac{C(s)}{1 + C(s)P(s)} \tag{3.12}$$

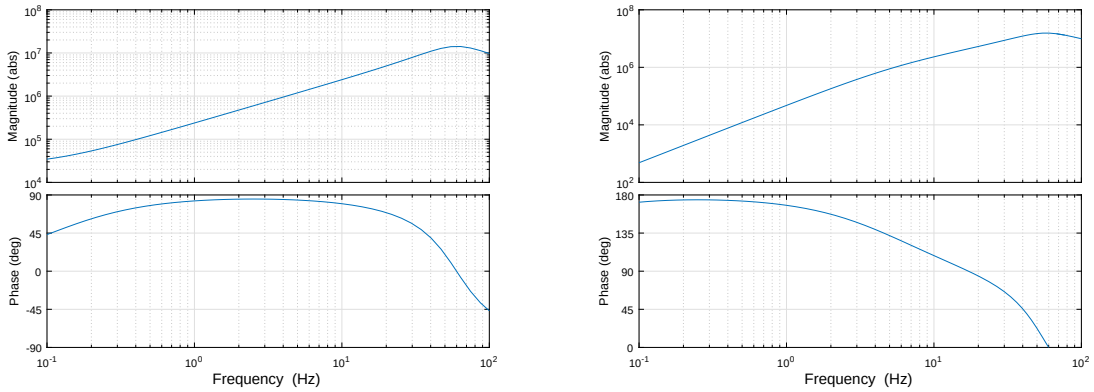

(a) Noise sensitivity of the controlled system *(b) Noise sensitivity of the controlled system*

Figure 3.25: Comfort levels before and after calibration at different velocities

Looking at the bodeplots of the controller and the noise sensitivity it is clear that high frequency errors, 10-50 Hz, result in a high controller output, F. For example a position error noise of amplitude 0.1 mm with a frequency of 35 Hz, which is not uncommon, will be amplified by 1×10^7, resulting in a force

of 1000 N. Divided by the mass gives an acceleration ripple of amplitude $1\,\mathrm{m/s^2}$. That is why it is important to reduce the noise sensitivity at these frequencies. Two options will be discussed:

1. Decreasing the bandwidth
2. Adding a low-pass filter

3.3.1.1. Decreasing the bandwidth

What happens if the differential gain is lowered? Then there will be more overshoot and the controller needs more time to settle, or in other words, the system becomes less stable. So if the D gain is to be lowered then so should the P gain, which basically means lowering the bandwidth. It is expected that this will reduce the amplification of noise, but the downside is that the position tracking error will increase due to the lowered proportional gain. This is not a huge problem when the car is moving, but when it is about to land, it will have a large error to correct.

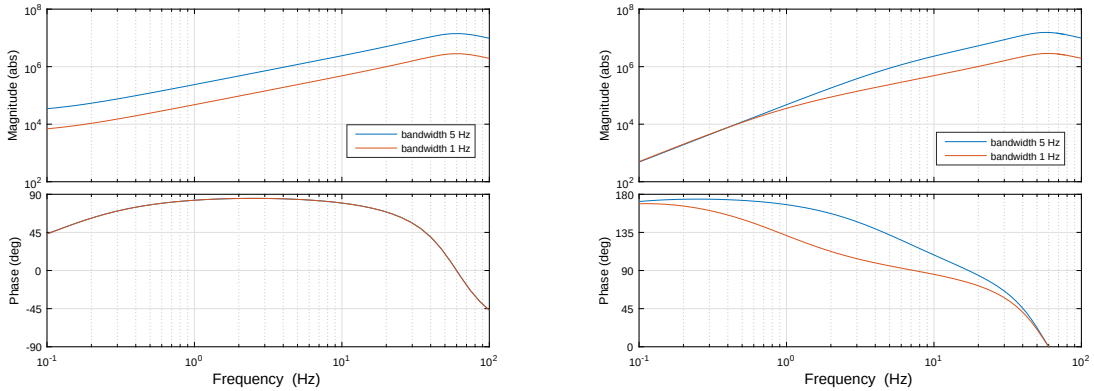

(a) Controller of the controlled system *(b) Noise sensitivity of the controlled system*

Figure 3.26: System bode plots at different bandwidths

Reducing the bandwidth by a factor 5 also reduces the amplification by around a factor 5. Figure 3.27 shows the positive effect this has on the comfort.

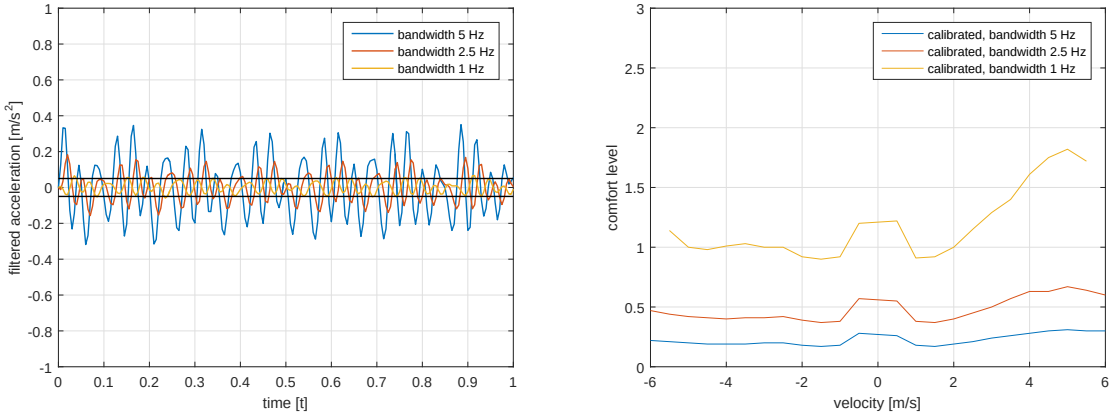

(a) Acceleration ripple *(b) Comfort level for all velocities*

Figure 3.27: Effect of controller bandwidth on comfort level

The effect on comfort is also a factor 5. So in order to increase the comfort the bandwidth should be decreased. However there is a lower limit on the bandwidth, because decreasing it too much will eventually result in position tracking errors exceeding safety limits. Lowering the bandwidth will also

increase the sensitivity to disturbances, therefore a bandwidth of 1 Hz is chosen. Average and extreme values for different bandwidths are shown in Table 3.20.

Table 3.20: Average comfort level of the baseline and after calibration

	Comfort level		
Configuration	Min	Average	Max
Calibrated, 5 Hz	0.17	0.23	0.31
Calibrated, 2.5 Hz	0.37	0.48	0.67
Calibrated, 1 Hz	0.90	1.18	1.82
Uncalibrated, 1 Hz	0.67	0.98	1.70

3.3.2. Low-pass filter

The differential gain should be tamed, [21]. In the old controller this was done by a second order low-pass filter acting directly on the sensor output. Its cut off frequency is 50 Hz, which is much higher than the bandwidth frequency. According to [21], taming frequencies should be around 3 times the bandwidth frequency. To decrease the noise sensitivity the differential gain is tamed at a frequency, f_t of 4 Hz, Equation (3.13), and the bandwidth stays at 1 Hz, leading to the bodeplots in Figure 3.28.

$$C(s) = K_p + \frac{K_d s}{\frac{1}{\tau_t s + 1}} \qquad \tau_t = \frac{1}{f_t \cdot 2\pi} \tag{3.13}$$

(3.14)

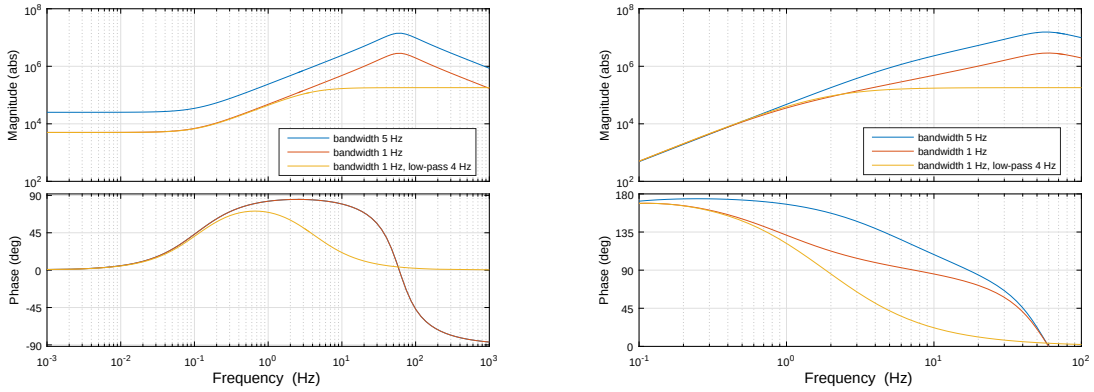

(a) Controller of the controlled system *(b) Noise sensitivity of the controlled system*

Figure 3.28: System bode plots with and without an extra low-pass filter

As expected at frequencies higher than 4 Hz, the controller gain and noise sensitivity gain are considerably lower, than without the extra taming of the differential gain. It was expected that with this extra low-pass filter, the vibrations will be lower. Because the noise frequency rises with velocity, it was also expected that the effect is highest for higher velocities. Figure 3.29 shows that this expectation is totally wrong.

Figure 3.29a shows that higher frequencies are indeed attenuated, but a negative side effect is triggered. The extra settling time required for the controller is the cause of this side effect. The new lower frequency vibration is triggered every time the actuation is handed over between motor controllers. Section 3.3.3 will collaborate on this effect and propose a solution.

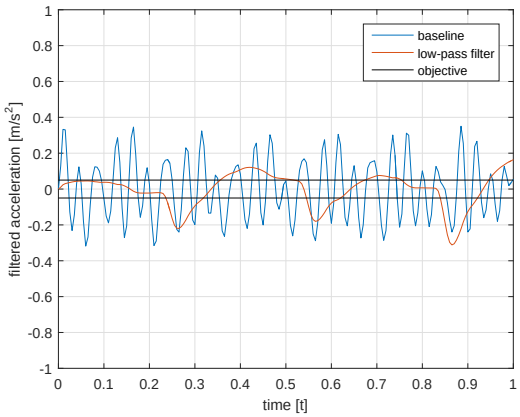

(a) Acceleration ripple

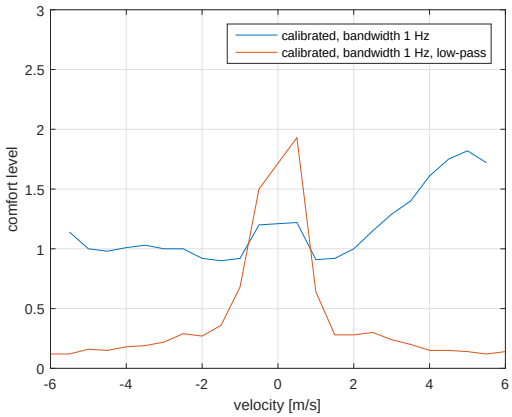

(b) Comfort levels

Figure 3.29: Effect of a low-pass filter on comfort level

Table 3.21: Average comfort with and without extra low-pass filter

	Comfort level		
Configuration	Min	Average	Max
Calibrated, 1 Hz	0.90	1.18	1.82
Calibrated, 1 Hz with low-pass filter	0.12	0.37	1.93

3.3.3. Feedback window

Taming the differential gain is a must in order to reduce vibrations. However it is observed that at higher velocities a negative side effect becomes dominant. In Section 2.2.1.5 the handing over of controllers was discussed. Every control has only a limited time to settle on the correct feedback force. When only proportional and differential control is applied settling is immediate. The controller receives a position and a velocity error and they are multiplied by their gains to reach the controller output. But without filtering the velocity error is very noisy and large vibrations are the result. So a filter is required, but a low-pass filter introduces a settling time for the controller, Figure 3.30.

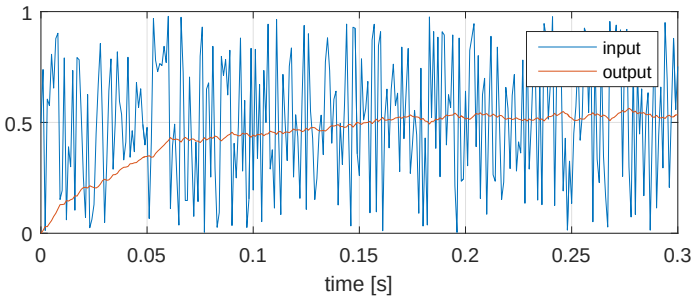

Figure 3.30: A low-pass with a cut-off frequency of 4 Hz *needs* 0.13 s *to settle*

In the current configuration of handing over the control, controllers have 0.15 m to settle. So at a velocity of 4 m/s this means less than 0.04 s are available for settling. This explains the bad performance of the designed low-pass filter. One solution is to increase the available settling time. That is achieved by reducing the amount of controllers used for feedback, Figure 3.31, Table 3.22. Feed forward can still be applied by 7 or 8 controllers, but only 5 or 6 controller will be used to apply feedback. Because the feedback force is small relative to the feed forward force, 5 controllers are sufficient to provide this. A separate windowing algorithm is created to deal with this. It was chosen to make the feedback window symmetrical for ease of implementation and redundancy reasons. This means that the first and last controller covered by the magnet yoke only provide feed forward and the 5 or 6 controllers in between apply both a feedback and a feed forward force. This increases the settling distance by 0.3 m.

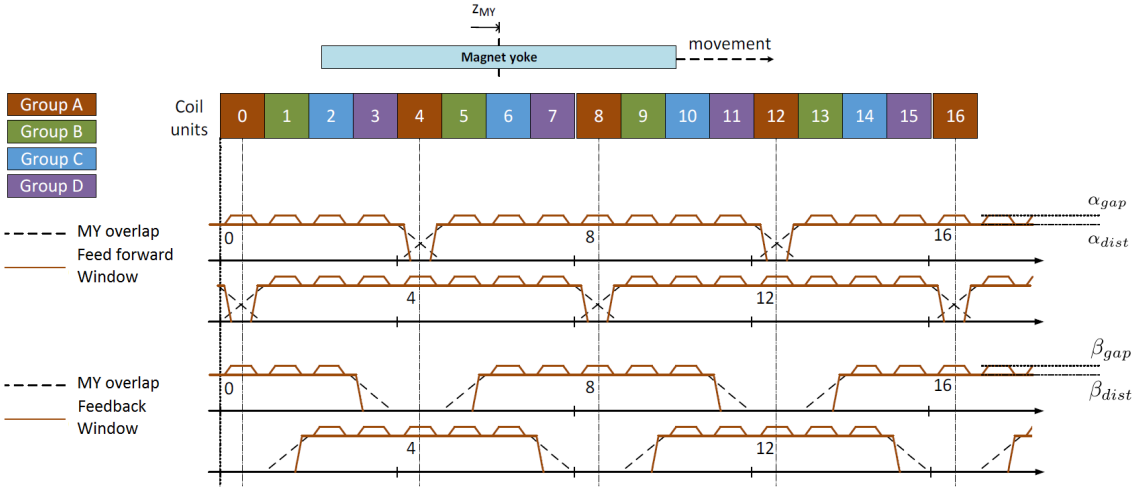

Figure 3.31: With and without feedback window

Table 3.22: Windowing parameters

Symbol	Description	value
α_{dist}	Distributed control gain	0.125
α_{gap}	Compensation gain	0.143
β_{dist}	Distributed control gain	0.167
β_{gap}	Compensation gain	0.2

As expected the comfort is improved compared to the previous windowing configuration, Figure 3.32. However the settling time required by the controllers was still too big for available distance that was created by the new window. An overview of the results is given in Table 3.23.

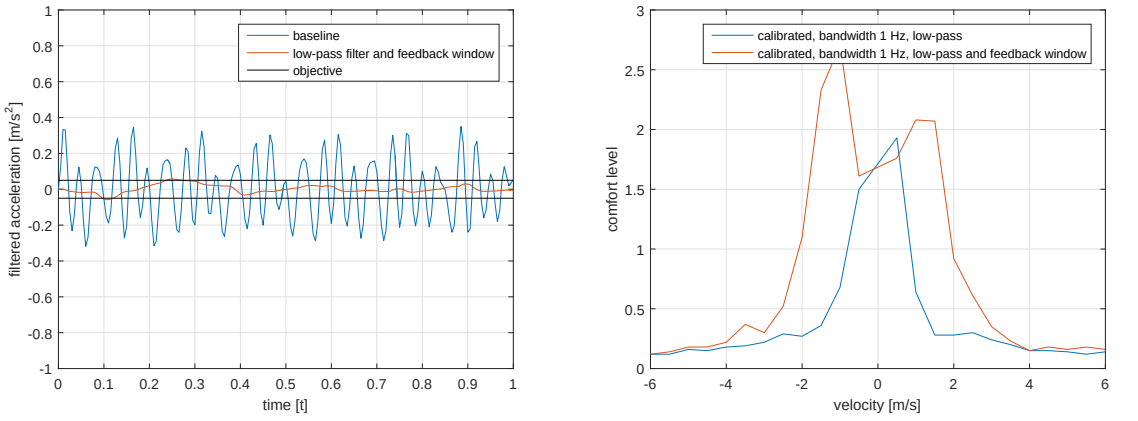

(a) With and without feedback window

(b) Low-pass filter, with and without feedback window

Figure 3.32: Effect of a low-pass filter and a feedback window on the comfort level

3.3.4. Final result vertical track

When the demand velocity is known it is possible to chose either control configuration based on the best comfort level at that velocity. With this switching of control a comfort level higher than 1 can be achieved for all velocities, except 2 m/s. On average an improvement of over 650% is made and the objective is achieved.

Table 3.23: Comfort levels achieved by the feedback window

	Comfort level		
Configuration	Min	Average	Max
Calibrated, 1 Hz with low-pass filter	0.12	0.37	1.93
Calibrated, 1 Hz with low-pass filter and feedback window	0.12	0.78	2.71
Calibrated, 1 Hz with feedback window	0.80	1.19	1.74

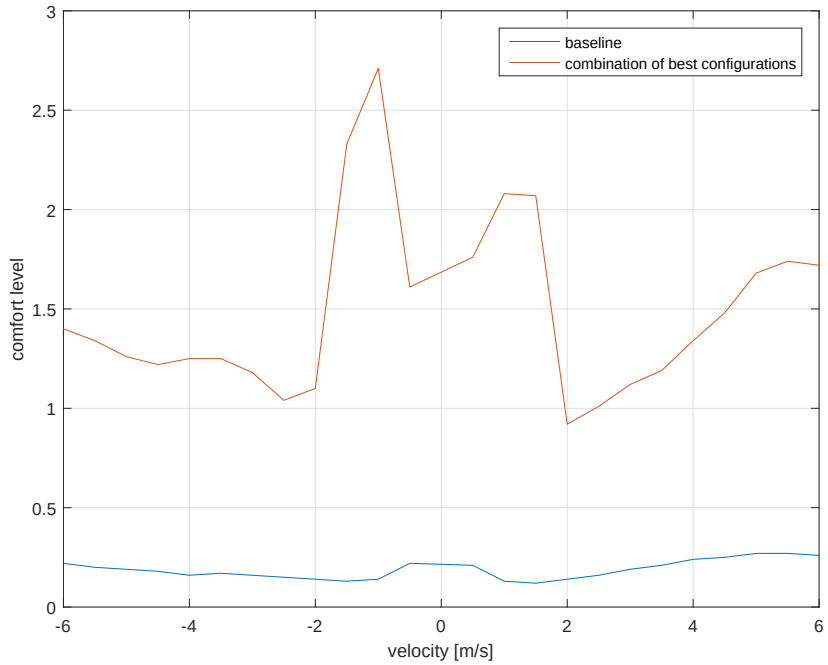

Figure 3.33: Comfort level of the combination of best configurations

Table 3.26 shows an overview of the comfort levels achieved by all different solutions and combinations.

Table 3.24: Overview of achieved comfort levels on the vertical track

	Comfort level		
Configuration	Min	Average	Max
Baseline	0.12	0.19	0.27
Calibrated, 5 Hz	0.17	0.23	0.31
Uncalibrated, 1 Hz	0.67	0.98	1.70
Calibrated, 1 Hz	0.90	1.18	1.82
Calibrated, 1 Hz with low-pass filter	0.12	0.37	1.93
Calibrated, 1 Hz with low-pass filter and feedback window	0.12	0.78	2.71
Combination of best configurations	0.92	1.49	2.71

3.3.5. Final result horizontal testtrack

A final controller is developed with insights gained from previous tests. These adaptions were made:

- Higher cut off frequencies for the low-pass filters
- Position sensor clipping based on feedback window
- Magnet yoke correction, discussed in Section 3.2.3

Table 3.25 shows the most prominent differences made in the controller.

Table 3.25: Prominent differences between baseline and final optimized controller

Parameter	Baseline	Optimized controller	Unit
Controller bandwidth	5	1	Hz
Low-pass filer cut off frequency	-	5	Hz
Motor controllers used for feedback	7-8	5-6	
Sensor range for feedback	1.23	1.1	m
Magnet yoke correction	no	yes	
Position sensor calibration	no	yes	

Higher cut off frequency

It is observed that taming the differential gain resulted in a higher settling time. Increasing the cut off frequency to 5 Hz decreased the settling time. In combination with a smaller position measurement range the handing over between controllers is improved.

Clipping of position measurement

The range of the feedback window is reduced to 0.9 m on both sides of the coil unit. That means the range of the position measurement can be reduced. $\frac{de}{dz}$ is highest at the ends of the sensor range. These ends are not required for the feedback window, so they are clipped, Section 3.3.5.

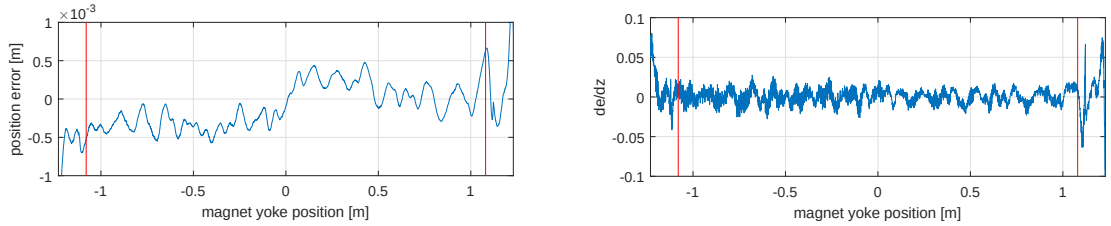

(a) Position error *(b) Derivative of the position error*

Figure 3.34: The range of the sensor is clipped where the derivative of the position error is greatest

Sensor clipping does decrease the available settling time for the controller, but the settling error becomes much smaller. In combination with the increased cut off frequency and the magnet yoke correction the comfort level is improved even more.

3.3.5.1. Comfort

The optimized controller is only tested on the horizontal track. Vibrations and comfort levels are shown in Figure 3.35.

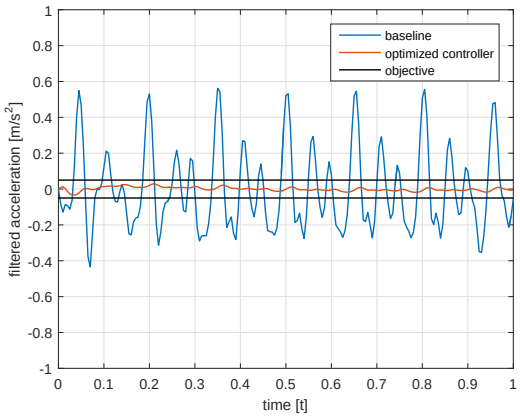

(a) Filtered acceleration

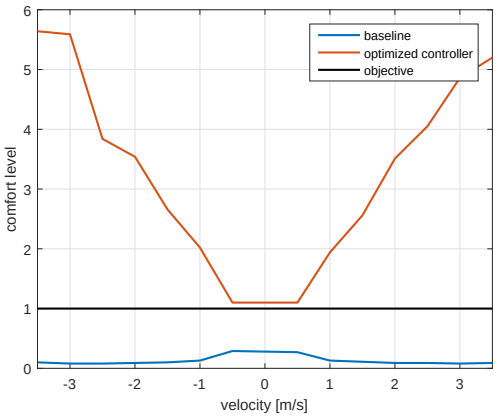

(b) Comfort values

Figure 3.35: Comparison of the baseline with the optimized controller

With this controller the objective is achieved for all velocities. The low-pass filter performs better as the velocity increases as is expected. Handing over of the controllers is optimized by clipping the range of the position sensor for feedback. Table 3.26 shows an overview of all configurations and their comfort levels.

.

Table 3.26: Overview of achieved comfort levels on the horizontal track

	Comfort level		
Configuration	Min	Average	Max
Baseline	0.08	0.12	0.29
Magnet yoke correction	0.12	0.17	0.33
Calibrated	0.10	0.15	0.30
Calibrated and magnet yoke correction	0.20	0.25	0.39
Optimized controller	0.81	1.51	2.43
Optimized controller, magnet yoke correction	0.93	2.76	4.71
Optimized controller, calibrated	0.88	1.68	2.37
Optimized controller, calibrated and magnet yoke correction	1.10	3.40	5.64

4. Discussion

4.1. Error analysis

In the first part of this research the causes of discomfort were investigated. This resulted in the quantification of each factor's contribution to the vibrations. The improvements that were made on the position sensor and on the controller were based on these findings. Most analysis was done in simulations, but measured values were used as input. The acceleration ripple that was simulated showed a big resemblance to the measured ripple. This indicates that the results of the error analysis are reliable. Some values were not based on measurements but on estimations, for example the damping uncertainty. Because all influences were minimal compared to the influence of the position sensor, the correctness of these estimations is irrelevant.

4.2. Calibration

4.2.1. HS bias

Correcting the bias of the every individual Hall sensor is a success. In combination with the correction of the sensitivities it lead to an improvement of the comfort of more than 15%. On top of that, it enabled using a correction model for the magnet yoke.
A precision of less than 5% was found between two measurements. These measurements were performed with a time interval of three weeks. Larger time intervals will have to be taken to be sure that the bias does not change with time.
The method used in this research could be replaced by a measurement that measure the bias an the sensitivity simultaneously. Data has shown that these methods differ only by 1%.

4.2.2. HS sensitivity

Calibrating the sensitivity of the Hall sensors is also a success. The difference in relative sensitivity was smaller than 4×10^{-3} for 95% of the measurements, so that is the achieved precision. In combination with the bias correction it created almost identical position errors.
The variance over time has not been researched to the full extend. If measurements show that the values change over time, a periodic calibration is required. The method used in this research is suitable to do this on site.
If the sensitivity of the Hall sensors does not change, the sensors could be calibrated before implementation.

4.2.3. Magnet yoke correction

The successful calibration of the Hall sensors enabled the creation of a correction model for the magnet yoke. After implementation the correction model reduced the position error from$0.7\,\mathrm{mm}$ to $0.2\,\mathrm{mm}$. This had a positive effect on the acceleration ripple, it was decreased to 20% of its original value.
Implementing the magnet yoke correction is easy for a system with only one magnet yoke. As the number of yokes increases, it will require more bookkeeping and more controller memory. The alternative is to improve the manufacturing process of the magnet yoke. Expectations are that due to the tolerances of the magnets a position error will remain, so a correction will have to be implemented to achieve desired comfort levels.
During this research the correction model is created by comparing individual position sensor data to an averaged signal. The average also contains errors, but if this process is iterated a more accurate correction model could be found. For now the result is sufficient, but for future systems this might come in use.

4.3. Control

4.3.1. Bandwidth

Lowering the bandwidth resulted in the biggest increase in comfort. The downside of lowering the bandwidth was the bigger position error. By switching between a landing and a trajectory controller, a comfortable ride with a small final position error is achieved.
One could argue to decrease the bandwidth even more, but safety and redundancy regulations do not allow this. A maximum position tracking error of $0.1\,\mathrm{m}$ is allowed, bigger errors will negatively affect the windowing algorithm. Passengers can jump or cause other external forces, this also puts a limits the minimum bandwidth.

4.3.2. Low-pass

Some filtering was done by the observer at a cut off frequency of $60\,\mathrm{hz}$. Analyzing the control sensitivity showed that a lower cut off frequency was required. Using rules of thumb and simulation results a second order low-pass filter was created with a cut off frequency of $4\,\mathrm{hz}$. This low-pass was successful in simulations and on the horizontal track. But in the vertical shaft, where higher speeds were possible it failed at speeds above $2\,\mathrm{m/s}$.
After more research the reason for this failure was discovered. The controllers need more time to settle when a low-pass filter is applied, this effect becomes visible at higher velocities. A higher cut off frequency, clipping of the position sensor range and the introduction of the feedback window solved this issue.

4.3.3. Feedback window

For energy efficiency reasons, it is desired to use as many controllers at the same time as possible. This holds for the feed forward force, but the feedback force needs to provide stability and not all available motors are required to provide this stability. The implemented feedback window reduced the amount of controllers used for feedback from 8 to 6. This provides the controllers with more time to settle, which is needed when a low-pass filter is used. In combination with the low-pass filter a big improvement was made for velocities below $2\,\mathrm{m/s}$, but at higher velocities the settling time was still too big.
Currently the window excludes the first and last coil unit overlapped by the magnet yoke. This symmetry was chosen for the ease of implementation and smoothness. Better results might be obtained when only the last or last two coil units are excluded.

4.3.4. Final controller

A final controller is designed after analyzing the results from the first experiment. It is tested only on the horizontal track, but the results are very promising. Because of the great similarities between results on both tracks, it is expected that similar comfort levels can be achieved in the vertical shaft as well.

4.3.4.1. Improved low-pass filter

Knowledge obtained with the first tests, has led to the improvement of the low-pass filter. It was observed that the filter introduced a ripple at velocities higher than $2\,\mathrm{m/s}$. Increasing the cut off frequency of the filter reduced the settling time and resulted in a higher comfort level for the higher velocities.
An even better result could be obtained if the cut-off frequency of the low-pass filter is dependent on the velocity. At low velocity the available settling time is bigger, so a lower cut-off frequency would suffice. Then as the velocity increases the cut-off frequency should increase proportionally.

4.3.4.2. Sensor clipping

The position sensor is the least accurate in the beginning and end of its range. Differentiating to obtain the velocity results in even bigger errors in these sections. With the implementation of the feedback window the range of the position sensor can be decreased. This means there is even less time to settle, but the velocity measurement becomes much more accurate. Optimizing this trade-off has resulted in even higher comfort values.

4.4. Acceleration measurement

This research has focused on the discomfort caused by the propulsion system. The acceleration ripple is the cause of discomfort. An accelerometer measures all acceleration, also vibrations that are not caused by the propulsion system. For example those caused by dynamic behavior of the car or because of imperfect wheels. On the other hand when a force signal is used to calculate acceleration, the characteristics of the actuator are not considered. Both methods have been used on the baseline measurement and based on the similarity the conclusion was drawn, that the second method is appropriate to measure the comfort level as a result of the propulsion system. Because of international elevator standards, [5], a measurement with the accelerometer is required to establish the real comfort levels of the system. It is expected that the comfort level will not differ much from this research method.

5. Conclusions

Worlds first ropeless elevator will only be a success if people enjoy their ride in it, ride comfort is an essential aspect of passenger's experience. Before this research comfort levels were 5 times lower than that of traditional elevators. In order for this innovative system to be a commercial success, this level needs to be improved, a level of 1 is set as the objective. Vibrations are the cause of discomfort, but up to this research there were only speculations about the causes of these vibrations.

This research has resulted in a quantified overview of all the sources of vibration, the most dominant source being noise of the position sensor. Measurements and simulations have also provided insight in the noise characteristics of this sensor. The sensor's position error is reduced by 75%, by means of calibration and a correction model. This reduction of the error improves comfort levels by 108%.

Still comfort levels are below the desired value. The controller is optimized to deal with the remaining sensor noise and the challenges of distributed actuation. A first prototype is tested on a vertical track and comfort levels higher than the objective are achieved. However not for all velocities. A second controller, improved based on experimental data from the first prototype, is tested on a horizontal track and the objective is beaten by a factor 3 on average. Tables 5.1 and 5.2 show the achieved average comfort levels and the improvement with respect to before this research. Because both tracks are almost identical, it is expected that similar comfort levels will be achieved on the vertical track

It can be concluded that the successful development of a calibration program, a correction model and an optimized controller has achieved and exceeded the objective. Ride comfort of ropeless elevators has reached the level of traditional elevators.

Table 5.1: Achieved improvement on the vertical track (objective is a comfort level of 1)

	Average comfort level	Improvement %
Baseline	0.19	0%
Calibration	0.23	18%
Control	0.98	368%
Control and calibration	1.19	529%

Table 5.2: Achieved improvement on the horizontal track (objective is a comfort level of 1)

	Average comfort level	Improvement %
Baseline	0.12	0%
Calibration	0.15	25%
Magnet yoke correction	0.17	42%
Calibration and magnet yoke correction	0.25	108%
Control	1.51	1158%
Control and calibration	1.68	1300%
Control and magnet yoke correction	2.76	2200%
Control, calibration and magnet yoke correction	3.40	2700%

5.1. Future research and recommendations

Comfort levels for the system that was investigated during this research are improved to exceed acceptable levels, but it is yet unknown if the maximum comfort has been achieved. Also more systems will follow, dealing with similar issues.

5.1.1. Calibration

The bias and sensitivity of the Hall sensors were measured only twice during this research. It is yet unknown if they are constant over time. More research is required to investigate how these values change over time. If this is the case, a periodic calibration algorithm is required. The algorithms used

in this research are capable of doing this. If however the Hall sensors remain the same with respect to time, one calibration before implementation suffices. Research could be done in how to achieve this during the production of the position sensors.

5.1.2. Magnet yoke

A relatively large error is caused by the tolerances of the magnet yoke. The correction model is able to reduce this error. But for future systems it could be profitable to improve the manufacturing process of the magnet yoke.

5.1.3. Low-pass filter

With the filter of the final controller, high comfort values are achieved at high velocities. Due to the relatively high cut-off frequency with respect to the noise frequencies at low velocity the comfort values are lower for these velocities. Research in a velocity dependent low-pass filter can result into higher comfort values over the entire velocity operating range of the elevator.

5.1.4. Feedback window

The designed feedback window is symmetrical, due to the ease of implementation. An asymmetric window could provide more available settling time for the motor controllers.

5.1.5. Comfort evaluation

Comfort levels of the system have been evaluated using a force input signal. Acceleration measurements according to international standards are required for the development of an official ride comfort report.

Appendix A. Hall effect sensor

When a magnetic field is held close to a current carrying conductor, charged particles are forced in a direction perpendicular to the magnetic field. The voltage difference between the opposing sides can be measured with a volt meter. If the sensitivity is known, the magnetic field can be deducted from the measured voltage, Figure A.1.

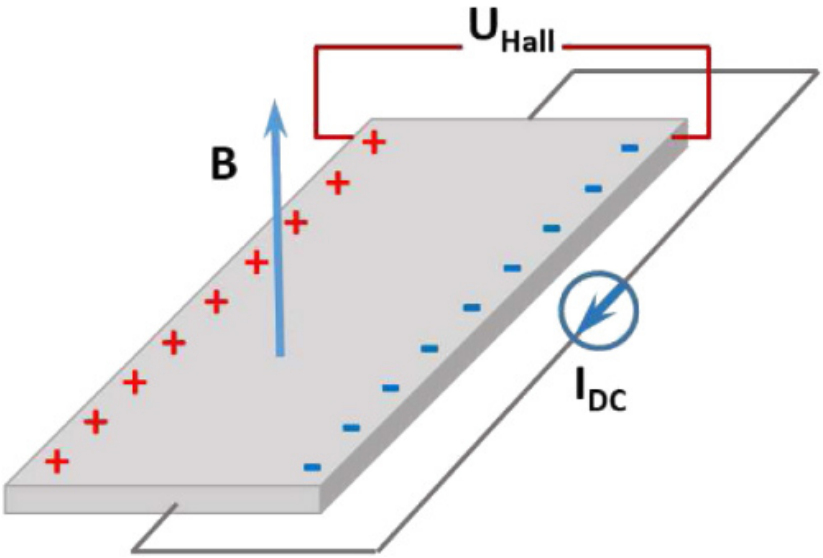

Figure A.1: Working principle of a Hall effect sensor

Material properties and manufacturing can result in a small bias voltage over the volt sensor. For the same reasons sensitivities are different between different Hall sensors.

Appendix B. Control sensitivities and stability analysis

B.1. Open loop stability

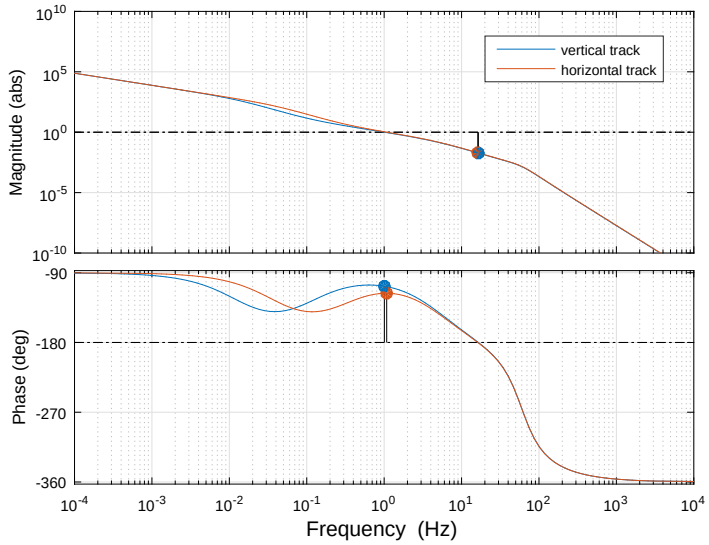

Figure B.1: Open loop sensitivity

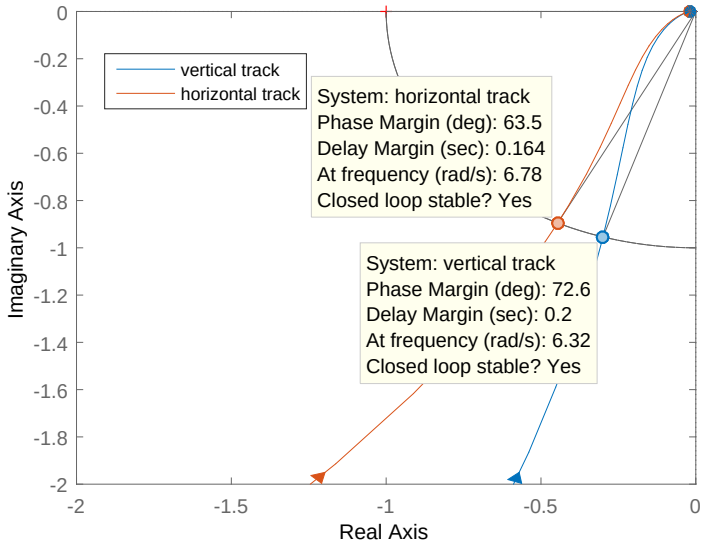

Figure B.2: Stability margins represented in a nyquist plot

B.2. Sensitivity

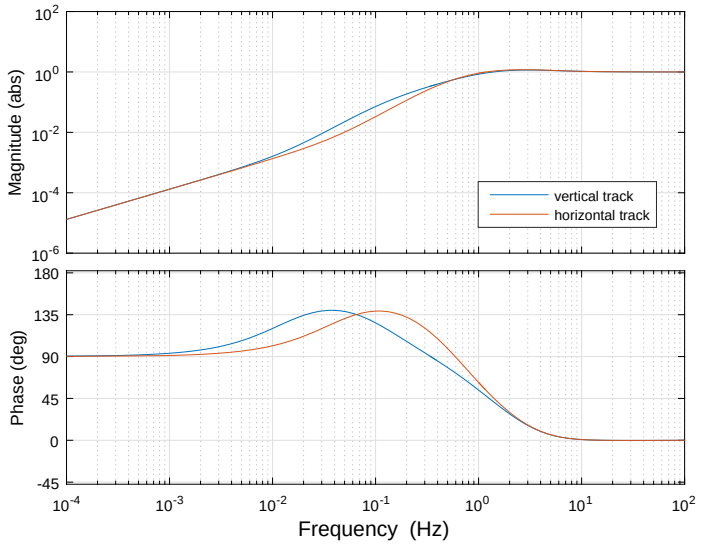

Figure B.3: Sensitivity, disturbance rejection

B.3. Complementary sensitivity

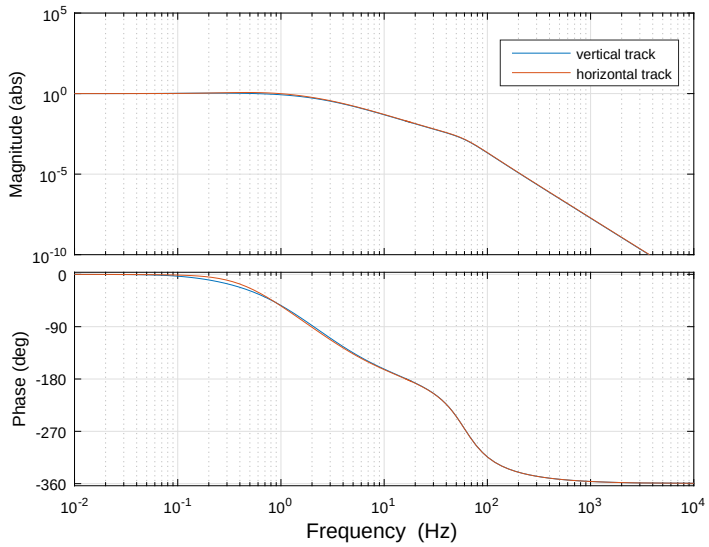

Figure B.4: Complementary sensitivity, noise rejection

B.4. Process sensitivity

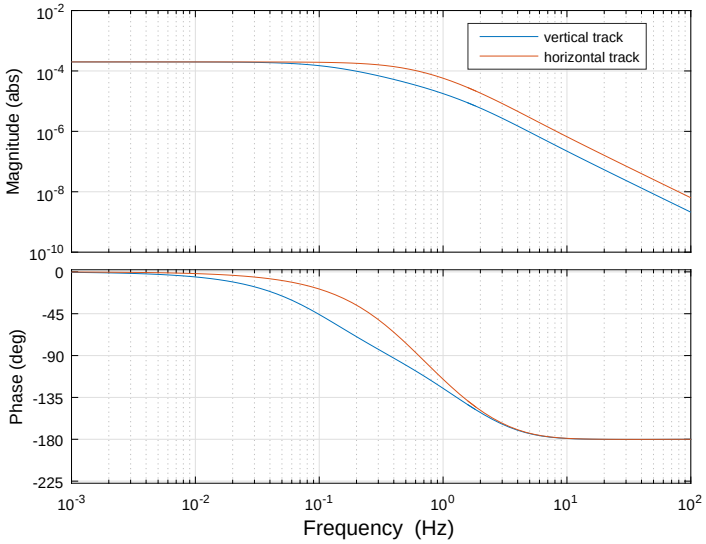

Figure B.5: Process sensitivity,

Appendix C. Calibration

This appendix describes the algorithms that were used to obtain the Hall sensor bias and sensitivity values.

C.1. Hall sensor biases

Every Hall sensor should have the same output voltage when no magnetic fields is present, in theory. The difference from this value is called the bias, which is caused by manufacturing, material and other imperfections. In the design of the position sensor, more Hall sensors were used to minimize the effect of this small bias, but there is still a position error due to this effect. Fortunately it is relative easy to measure the bias, this enables calibration. In Figure A.1 the working principle was shown.

C.1.1. Measurement

The magnetic field measured by every single Hall sensor can be traced. When no magnet is in the proximity around the bias is measured during approximately $10\,\mathrm{s}$ with a sample frequency of $200\,\mathrm{Hz}$. An average of the retrieved data is taken and this results in a bias value for every Hall sensor. Figure C.1 shows that the biases are normally distributed, which was expected.

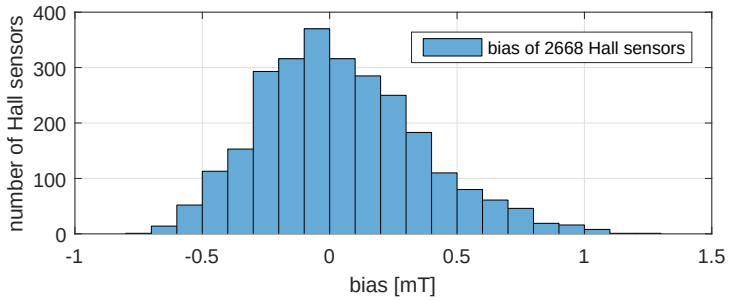

Figure C.1: The bias of 2688 Hall sensors

Table C.1: Hall sensor specifications: Allegro A1388

Specification	min	typical	max	unit [mm]
Offset voltage	2.488	2.500	2.512	[V]
Sensitivity	24	25	26	[mV/mT]
Output bias	-0.48	0	0.48	[mT]

A standard deviation can be deducted from the measurements, it is $0.31\,\mathrm{mT}$. This means that 95% of the Hall sensor biases lie between -0.62 and $0.62\,\mathrm{mT}$. This value is slightly higher than the specifications, but these valules are also influenced by the analog to digital converter and other additional components.

C.1.2. Repeatability

The measurement has been repeated several times to investigate the accuracy of the measurement and the effect of time. Values did not differ more than $0.02\,\mathrm{mT}$, which is smaller than the quantization value of $0.05\,\mathrm{mT}$. So it can be concluded that it is possible to measure and correct the bias with a precision of $0.05\,\mathrm{mT}$.

C.2. Hall sensor sensitivity

The sensitivity is the ratio between output voltage and the measured magnetic field strength. Similar reasons that applied to the bias are valid for the sensitivity of every Hall sensor. If only one hall sensor

is being used the sensitivity would not be a problem, but the algorithm requires at least 2 sensors. Using more will reduce the effect of individual differences, but an error will always remain. Again if the sensitivity can be measured it is possible to correct this value within the software of the sensor. However measuring the sensitivity required a more complex algorithm than the bias. This section will explain the algorithm that was used to measure and will discuss the results.

C.2.1. Measurement

Two algorithms are developed that could measure the sensitivity without having to remove the sensor.

1. An algorithm based on the peaks of the measured magnetic field
2. An algorithm based on the area under the measured magnetic field

Peak values

In order to measure sensitivity a constant magnetic field is required. The magnet yoke is used a reference for measuring the sensitivity. It consists of several magnets that do not change over time. So in theory every Hall sensor should measure the same field when the yoke is passing. The difference in measurements between Hall sensors is caused by the different sensitivities and small tolerances of the guiding system. By looking at the relative sensitivity within a group of 8 Hall sensors, the effect of the guidance tolerances is minimized. The fact that there are more magnets located on the yoke is an advantage, because it means more data is gathered every measurement. This algorithm is explained in a few steps:

1. Magnet yoke passes the position sensor with a constant velocity of $0.5\,\mathrm{m/s}$
2. Different Hall sensors measure a similar but slightly different alternating magnetic field, Figure C.2b
3. The average at each peak is taken, Equation (C.1)
4. For every selected peak a relative sensitivity is calculated, Equation (C.2)
5. The final relative sensitivity is obtained by taking the average at every measured peak

$$B_{peak,average} = \frac{\sum_{i=1}^{n} B_{peak,i}}{n} \tag{C.1}$$

$$\mathcal{S}_i = \frac{B_{peak,average}}{B_{peak,i}} \tag{C.2}$$

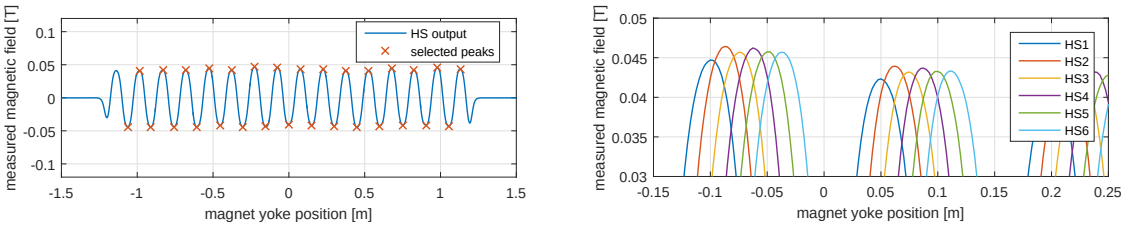

(a) Peaks used to calculate sensitivity

(b) 6 Hall sensors provide 6 similar measurements

Figure C.2: Using the peak values to calculate the sensitivity

An equal amount of positive and negative peaks are used to determine the sensitivity in order to get rid of the effect of the bias. The lower the speed of the magnet yoke, the higher the accuracy. $0.5\,\mathrm{m/s}$ was chosen, because it results in about 1000 data points over a range of $2.5\,\mathrm{m}$, which means a resolution of $2.5\,\mathrm{mm}$. A smaller resolution would increase the measurement time. An advantage of this algorithm is the possibility to compare sensitivities values obtained at different peaks. The deviation is an indication of the precision of the algorithm, Figures C.3a and C.3b show the measured

sensitivity and the deviation found between peaks. From this can be concluded that the sensitivity can be found with a precision of less than 4×10^{-3}. It can be also seen that the sensitivity is according the specifications.

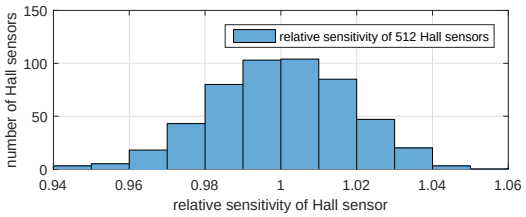

(a) Peaks used to calculate sensitivity

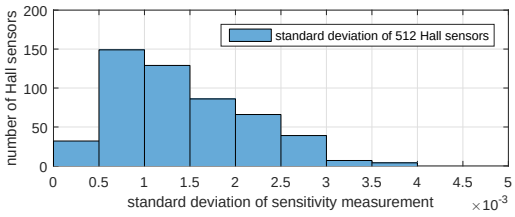

(b) 6 Hall sensors provide 6 similar measurements

Figure C.3: Using the peak values to calculate the sensitivity

Area

The previous algorithm requires a lot of post processing time. On top of that it uses only 2% of all the available data. When every point is evaluated according to previous algorithm, divisions by very small numbers can occur. This can lead to unreal values and also negative sensitivities. So instead of looking at every data point individually this algorithm looks at all data combined:

1. Magnet yoke passes the position sensor with a constant velocity of $0.5\,\mathrm{m/s}$
2. The average of the signal is subtracted to account for the bias
3. The signal is cut at a treshold of $3\,\mathrm{mT}$, three times the maximum bias
4. For every hall sensor the absolute area is calculated, Equation (C.3) and **??**
5. The area is compared with the average sensor group area to find the sensitivity, Equation (C.4)

$$\boldsymbol{B_{sum,average}} = \frac{\sum_{i=1}^{n} \boldsymbol{B_{sum,i}}}{\boldsymbol{n}} \tag{C.3}$$

$$\boldsymbol{\mathcal{S}_i} = \frac{\boldsymbol{B_{sum,average}}}{\boldsymbol{B_{sum,i}}} \tag{C.4}$$

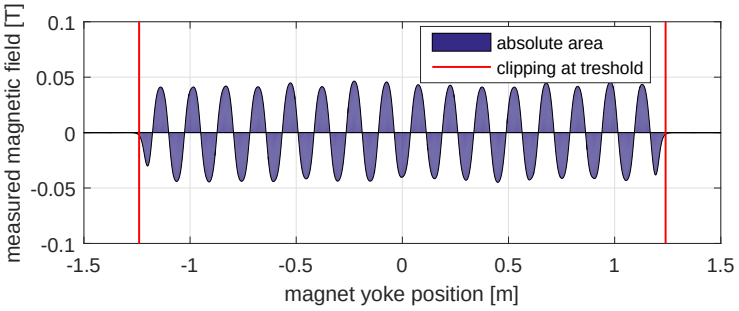

Figure C.4: The area under the Hall sensor signal, only the area between the red lines is taken into consideration

Subtracting the average is permitted, because the average of the magnetic field of the magnets should be zero, same amount of north and south poles. The standard deviation of the different algorithms applied on all sensors is 1.8×10^{-3}, Figure C.5b. This proves that both methods are successful and can therefore be applied. Because this algorithm is faster and requires less work, it is prefered.

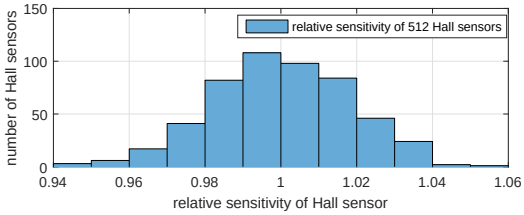

(a) Peaks used to calculate sensitivity

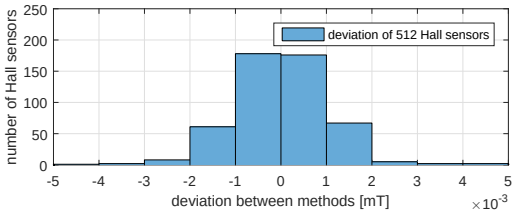

(b) 6 Hall sensors provide 6 similar measurements

Figure C.5: Using the peak values to calculate the sensitivity

Appendix D. System identification

In order to determine the open loop transfer function of the setup ,$P_ts(s)$, of the test setup, **??**, a system identification is performed. A pseudo random input force is used as an input for the system. The output is measured by the position sensor. With Matlab's function tfestimate a transfer function is estimated. This function is compared with the theoretical open loop, $L(s)$.

$$P_ts(s) = \frac{z_m}{F_{setpoint}} \tag{D.1}$$

$$P(s) = \frac{z}{F} = P(s) = \frac{1}{400s^2 + 105s} \tag{D.2}$$

The setups open loops transfer is shown in Figure D.1 together with the theoretical and estimated transfer function. The resulting estimated transfer function is given in Equation (D.3).

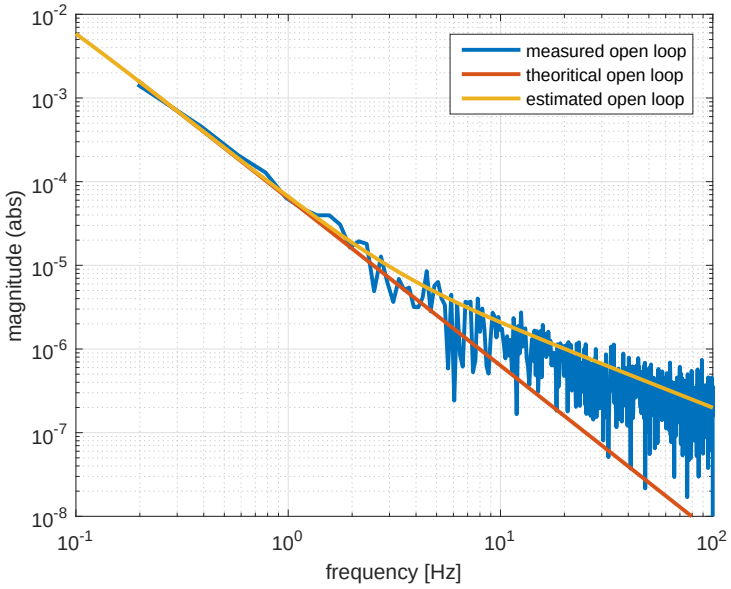

Figure D.1: Working principle of a Hall effect sensor

$$P_{est}(s) = \frac{0.05s + 1}{400s^2 + 105s} \tag{D.3}$$

Compared to the theoretic transfer function a zero is added. The reason behind this is unknown, but it adds phase at higher frequencies, which is beneficial for the system. From this system identification can be concluded that the transfer from force set point to applied force is indeed 1. Furthermore no unexpected disturbances or noises are present in the real system.

Appendix E. Instability due to current coupling

In Section 3.1.8.4 it is shown that current in the coils can cause a position error of the sensor. This position error will cause the feedback controller to apply more force, which might result in more current, Figure E.1. Equation (E.1) shows a simplified transfer function of this loop, , where $CU(s)$ is the transfer from a current to position error, $CC(s)$ is the transfer from force set point to current and $C(s)$ is the control transfer function. Because $CU(S)$ is non-linear, a simulation is used to investigate around which gain of the controller the system becomes unstable.

$$\frac{e_{zi}}{e_z} = \frac{C(s) \cdot CC(s) \cdot CU(S)}{1 - C(s) \cdot CC(s) \cdot CU(s)} \tag{E.1}$$

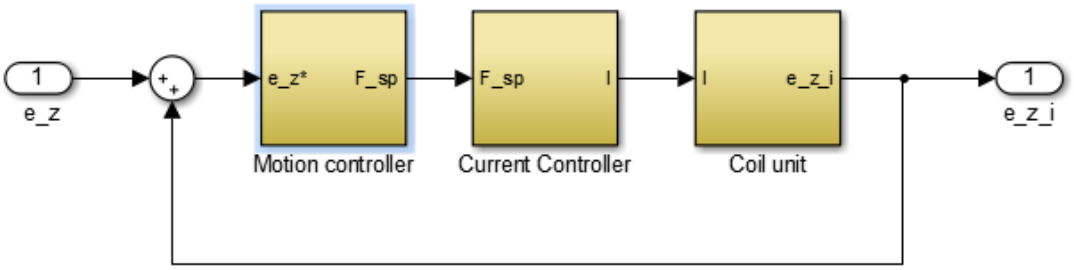

Figure E.1: Position error due to the coupled current of 60 A *of the neighboring coil unit*

This value was found to around 6×10^5 for a proportional gain. If the controllers gain stay well below this value it is expected that instability due to current coupling will not occur. In the simulation the magnet yoke is not affected by the increasing current, furthermore currents needed for feed forward control are also left out of consideration. Still it is important to know that instability can occur when the controller gain is too high.